chemosensors

MDPI

Review

New Trend of Amperometric Gas Sensors Using Atomic Gold-Decorated Platinum/Polyaniline Composites

Anifatul Faricha [1], Parthojit Chakraborty [2], Tso-Fu Mark Chang [2], Masato Sone [2] and Takamichi Nakamoto [1,2,*]

[1] Department of Information and Communications Engineering, Tokyo Institute of Technology, Yokohama 226-8503, Japan; anifatulfaricha@gmail.com
[2] Institute of Innovative Research, Tokyo Institute of Technology, Yokohama 226-8503, Japan; chakraborty.p.aa@m.titech.ac.jp (P.C.); chang.m.aa@m.titech.ac.jp (T.-F.M.C.); sone.m.aa@m.titech.ac.jp (M.S.)
* Correspondence: nakamoto.t.ab@m.titech.ac.jp

Abstract: The Amperometric Gas Sensor (AGS) uses an electrode as the transducer element which converts its signal into a current from the electrochemical reaction of analytes taking place at the electrode surface. Many attempts to improve AGS performance, such as modifying the working electrode, applying a particular gas-permeable membrane, and selecting the proper electrolyte, etc., have been reported in the scientific literature. On the other hand, in the materials community, atomic gold has gained much attention because its physicochemical properties dramatically differ from those of gold nanoparticles. This paper provides an overview of the use of atomic gold in AGSs, both in a bulky AGS and a miniaturized AGS. In the miniaturized AGS, the system must be redesigned; for example, the aqueous electrolyte commonly used in a bulky AGS cannot be used due to volatility and fluidity issues. A Room Temperature Ionic Liquid (RTIL) can be used to replace the aqueous electrolyte since it has negligible vapor pressure; thus, a thin film of RTIL can be realized in a miniaturized AGS. In this paper, we also explain the possibility of using RTIL for a miniaturized AGS by incorporating a quartz crystal microbalance sensor. Several RTILs coated onto modified electrodes used for isomeric gas measurement are presented. Based on the results, the bulky and miniaturized AGS with atomic gold exhibited a higher sensor response than the AGS without atomic gold.

Keywords: bulky AGS; electrode; miniaturized AGS; room temperature ionic liquid; isomers

Citation: Faricha, A.; Chakraborty, P.; Chang, T.-F.M.; Sone, M.; Nakamoto, T. New Trend of Amperometric Gas Sensors Using Atomic Gold-Decorated Platinum/Polyaniline Composites. *Chemosensors* **2024**, *12*, 27. https://doi.org/10.3390/chemosensors12020027

Academic Editors: Edward P. C. Lai and Michele Penza

Received: 25 December 2023
Revised: 1 February 2024
Accepted: 6 February 2024
Published: 12 February 2024

1. Introduction

Gas sensor technologies are extensively used for a wide range of applications, such as Heating/Ventilation/Air/Conditioning (HVAC) systems, the semiconductor industry, smart cities, security, environmental monitoring, the oil and gas industry, automotive and transportation applications, the medical industry, smart agriculture, etc. [1–4]. The market size of gas sensors reached $3.16 billion in 2022 and is projected to surpass approximately $6.2 billion by 2030 [1–4]. Furthermore, the Compound Annual Growth Rate (CAGR) is forecasted to grow around 8.81% from 2023 to 2030 [1–4]. The major factors driving the demand for gas sensors are sensor miniaturization coupled with the improvement of communication, networking, and wireless technology like the Internet of Things (IoT), cloud computing, big data, etc. [1–4].

There are many gas sensor types such as electrochemical sensors, semiconductor sensors, photoionization sensors, biosensors, etc. [1–4]. The semiconductor gas type is the most popular type, particularly to build the electronic nose system, but it requires a high-power consumption and typically its selectivity is lower than electrochemical sensors [5,6]. The biosensor type has a high selectivity by employing a certain living microorganism to detect the analyte; however, reproducibility and operating temperature become the issues [7]. Furthermore, with regard to the photoionization type, it has a high sensitivity, but it is relatively expensive [8,9]. Based on the report, the electrochemical (EC) sensor dominated the market share in 2022 with the

largest global revenue approximately 23.0% [1–4]. The high demand for EC sensors is due to this sensor type possessing a good selectivity coupled with less power consumption [1–4].

The Amperometric Gas Sensor (AGS) is one of the popular classes of EC sensor [10]. Numerous works have been performed to improve the catalytic activity of the AGS; one of the common ways is by modifying its working electrode (WE) using a catalyst [10–14]. In an AGS, a catalyst made from biological elements using a living organism offers high selectivity; however, the main issue is related to the short lifetime, and it cannot be operated at a high temperature [7]. On the other hand, nanoparticles (NPs) have been widely used as a catalyst for many years. Although NPs play a notable role as a catalyst, their catalytic activities depend on their size. Reduction to atomic cluster shows a remarkable catalytic activity [15,16].

According to numerous published reports, the physical and chemical properties of atomic gold clusters are dramatically different from those of gold NPs and bulk gold [11,12,15]. In an atomic gold cluster, the quantum and geometrical effects possessed by each atom contribute to its unique properties, such as the oscillation property known as odd-even pattern which NPs do not have. In addition, the catalytic activity shown by atomic clusters is much higher than gold NPs [14].

Atomic clusters are a promising catalyst for AGS. A higher sensor response can be achieved than using NPs due to the larger active area undergoing catalytic reactions. There are a number of research works using NPs for gas sensors [17–21]; however, the research related to atomic clusters for amperometric sensors is very limited [11–14,22–26]. In this paper, we describe how to fabricate an atomic gold cluster for gas measurement using a bulky AGS system. We further explain this research for a miniaturized AGS.

Sensor miniaturization is a promising technology development that principally offers numerous benefits in terms of response time, power consumption, portability, and chip integration. However, a low sensor signal is the main issue; hence, the atomic catalyst is indeed required to enhance the sensitivity. In the miniaturized AGS, Room Temperature Ionic Liquid (RTIL) was used as a substitute for the aqueous electrolyte due to fluidity and evaporation issues [27]. Although there are many works related to RTILs used for miniaturized AGSs [28,29], using atomic gold with the RTIL is still very new and can be explored. There have been no review papers of AGSs with atomic metal, although there is a good review paper of general AGSs [10].

Herein, the gas measurements using atomic gold-decorated AGSs for several volatile organic compounds (VOCs) are presented. We also provide our perspective to enhance the performance of miniaturized AGSs with atomic gold and RTILs.

2. Methodology

In this review paper, several related works were included which come from our previous works and other relevant research papers. Table 1 summarizes the main papers used in this manuscript including information like the keywords, references, and publication year.

Table 1. Relevant papers/works and keywords used in this review paper.

No.	Year [Ref]	Keywords
1.	2008 [10]	Amperometric Gas Sensor (AGS)
2.	2008 [10]	Electrolytes for AGS
3.	2020 [28], 2018 [30], 2014 [29], 2008 [11,31]	Room temperature ionic liquid in AGS
4.	2023 [19], 2022 [20], 2020 [32], 2017 [7], 2012 [18], 2010 [33]	Catalysts for AGS, i.e., biological elements, metal oxide nanostructures, metal nanoparticles, atomic metal
5.	2022 [34], 2018 [35], 2012 [15]	Atomic metal catalyst
6.	2020 [36], 2013 [21,37]	Polyaniline (PANI)

Table 1. *Cont.*

No.	Year [Ref]	Keywords
7.	2011 [12], 2012 [14], 2013 [22], 2016 [38], 2020 [23,26]	Atomic gold decorating PANI for amperometric sensors
8.	2008 [11], 2021 [39], 2023 [25]	Atomic gold with RTIL for AGS

In this review paper, firstly, some basic knowledge is provided regarding the working principle of AGSs with various electrolytes and catalysts. Then, the new sensing material related to the atomic metal properties is presented. Afterward, the experimental procedure to fabricate atomic gold on a bulky AGS is explained as well as the results of several VOCs in gas phase measurement. In a miniaturized AGS, RTIL can be used to substitute for the aqueous electrolyte. Several research publications are also explained briefly in Table 2 which includes both bulky and miniaturized AGS systems with atomic gold.

Table 2. Summary of conducted research works related to atomic gold for AGS.

AGS System	Year [Ref.]	Summary
Bulky AGS system	2020 [23]	■ building the atomic gold deposition system for a bulky AGS, ■ verifying the odd-even behavior for Pt/PANI/Au_N (where N = 1 to 4) in aqueous electrolyte (i.e., KOH); ■ target compound was propanol isomers measured in liquid and gas phase.
	2020 [26]	■ gas measurements using Pt/PANI/Au_2; ■ target compounds were alcohols, esters, ketones, and carboxylic acids.
Miniaturized AGS system	2021–2023 [25,39]	■ fabricating Pt/PANI/Au_2 on IDA electrode; ■ proposing RE using Ag/AgCl ink; ■ RTIL was [EMIM][Otf] only; ■ only one fixed EC potential explored; ■ target compounds were propanol isomers vapors only.
	2022–2023 [6,27,40]	■ fabricating Pt/PANI/Au_2 on several IDA electrodes; ■ three RTILs were explored, i.e., [EMIM][Ac], [EMIM][Otf], and [EMIM][Cl]; ■ several fixed potentials were investigated; ■ target compounds were gaseous butanol isomers; ■ finding the possible combination of RTILs and the fixed potentials to obtain a good discrimination capability among butanol isomers.

3. Amperometric Gas Sensors (AGSs)

3.1. Working Principle

An amperometric gas sensor (AGS) measures current as a sensor signal. AGSs are also well-known as amperostatic, polarographic, micro fuel cells, etc., but amperometry is the most popular name [10]. AGSs can be built using two- or three-electrode configurations. In an AGS, the three-electrode configuration shown in Figure 1 is commonly used because it uses the reference electrode to maintain a stable reaction and thus does not require calibrating to another electrode. Although the two-electrode configuration is simpler, the net voltage applied to the liquid depends on the current. We should avoid this situation. Figure 1 depicts the AGS with three electrode configuration, i.e., working electrode (WE), reference electrode (RE), and counter electrode (CE) where all the electrodes must be in contact with the electrolyte (a conductive solution) and connected to a potentiostat (either variable or constant potential can be used) [10]. Typically, an AGS uses a gas-permeable membrane to prevent electrolyte leakage and to filter the target gas (or analyte) flowing into the system [10]. The electroactive species of the target gas flowing into the AGS system undergoes the reduction and oxidation (redox) reaction when a suitable EC potential is

applied. The oxidation takes place at the anode (working electrode) and the reduction occurs at the cathode (counter electrode). The redox reaction which occurs at the CE and the WE can be determined in Equations (1) and (2), respectively [10].

$$O1^{n+} + ne^- \rightarrow R1 \quad \text{(reduction at CE as cathode)} \tag{1}$$

$$R2 \rightarrow O2^{m+} + me^- \quad \text{(oxidation at WE as anode)} \tag{2}$$

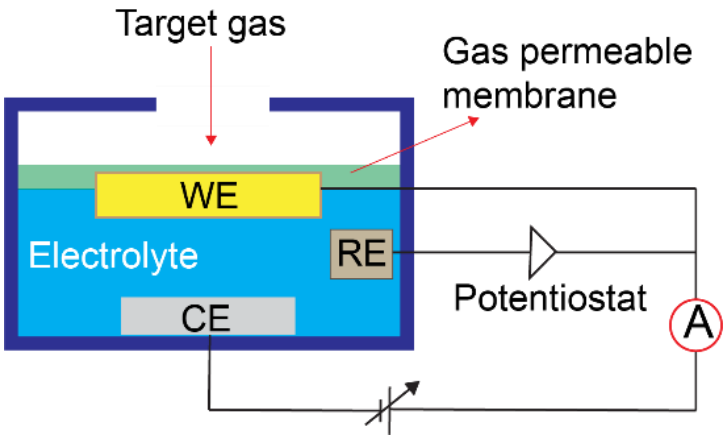

Figure 1. Illustration of AGS with three-electrode configuration. Reproduced from [6].

The reduction at the cathode (CE) contributes the electrons (e) which combine with the oxidized species ($O1$) to produce a reduced species ($R1$). At the same time, on the contrary, oxidation occurs at the anode (WE) where a reduced species ($R2$) generates the oxidized species ($O2$) and the electrons (e) are transferred to the WE. The charges are generated on each electrode surface; when an external circuit connects the WE and CE, then the electrons will flow from anode (WE) to cathode (CE) [10].

AGSs follow Faraday's law which can be briefly explained as follows: a number of electrons are generated from (at the WE) or consumed (at the CE) by an analyte, then the charge occurs on each electrode surface depending on the amount of the analyte taking part in the EC reaction at the electrode. Afterward, the current relies on the EC reaction rate which is directly proportional to the amount of analyte concentration. Consequently, in an AGS, the current is also proportional to the analyte concentration that can be measured between the WE and CE. The AGS generates a sensor signal when the analyte contains the electroactive species because it undergoes an EC reaction which either consumes or generates electrons (i.e., a redox reaction) [10].

For the electrodes, typically, the WE is made from a noble metal that is resistant to corrosion, such as gold or platinum. In addition, many forms of carbon are biocompatible; graphite and glassy carbon are also popular materials used for the WE [10]. Afterward, the CE is required to complete the circuit and must also be stable during the EC reaction; platinum is also generally used for the CE in an AGS. The RE is used to form a stable EC reaction and to avoid a voltage drop during measurement. Hence, basically, the RE should be not sensitive to relative humidity (RH), temperature, and other contaminants or reactants; Ag/AgCl is a very popular material used as the RE in the AGS, particularly in the three-electrode configuration [10,11,24].

There are numerous benefits offered by an AGS such as good selectivity, moderate cost, low power consumption, and good stability. Several methods can be conducted to improve the performance of AGSs such as modifying the WE, depositing a catalyst on the electrode, selecting the electrolyte, etc. An AGS provides the high electroanalytical performance at a modest price, thus making it a very popular choice for industrial applications. In addition, the sensor dimensions of an AGS are easy to miniaturize.

3.2. AGS with Various Electrolytes

The electrolyte is an ionically conductive medium which plays an important role in EC cells such as being the medium for the EC reaction, solubilizing the analyte, connecting all the electrodes, assisting the charge transport in the EC cell, etc. [10]. The electrolyte must be stable physically and chemically during the measurements for a long period. There have been three common types of electrolytes used in AGS systems, i.e., aqueous electrolytes, nonaqueous electrolytes, and solid electrolytes. Examples of aqueous electrolytes include sulfuric acid, potassium chloride, sodium hydroxide, acid, and base solutions. The nonaqueous electrolytes are propylene carbonate with lithium perchlorate, diethyl carbonate, tetrahydrofuran, etc. [10]. Furthermore, the solid electrolytes are the polymer Nafion, yttria-stabilized zirconia (YSZ), NASICON, β-alumina, etc. [10].

The AGS can operate from low to high temperatures which range from a temperature below freezing up to over 1000 °C and the material selections, including the electrolyte are also changed significantly. Generally, liquid electrolytes like aqueous and nonaqueous electrolytes operate at room temperatures and are commonly used for safety, industrial hygiene, and medical applications, whereas the solid electrolytes are used at a high temperature and are often used in stack gas process monitoring, automotive applications, internal combustion engine control systems, monitoring in harsh environments, etc. [10].

The aqueous electrolyte belongs to the liquid electrolytes. It is a water-based solvent including alkaline (base) and acid. Although in the 1970s nonaqueous and solid polymer electrolytes emerged for AGSs, the aqueous electrolyte is still favorable even nowadays due to its high conductivity, insensitivity to moisture, and good stability. The big companies like Figaro Engineering Inc. (Osaka, Japan) and Alphasense Inc. (Great Notley, Braintree, Essex, UK) are also still selling AGSs with an aqueous electrolyte. For example, the TGS 5042 for the detection of CO from Figaro Engineering Inc. uses a mixed alkaline electrolyte that consists of potassium bicarbonate ($KHCO_3$), potassium carbonate (K_2CO_3), and potassium hydroxide (KOH) [41]. The oxygen sensors products from Alphasense Inc. like the O2-A2 and O2-A3 sensors, also use a liquid electrolyte [42,43].

Although AGSs with liquid electrolytes have been used in many fields, the main issue encountered is the prolonged response time due to the presence of the gas-permeable membrane [10]. Therefore, it is impractical for sensing rapid changes of gas that occur within a second or less. Generally, aqueous electrolytes have a narrow EC potential window which limits the detection of a target gas which has redox reactions at a high EC potential. In addition, miniaturizing an AGS with a liquid electrolyte is hard to realize due to fluidity and evaporation issues since a gas permeable membrane is necessary to avoid electrolyte leakage and to slow down the evaporation rate of the electrolyte [10].

In this paper, we explain an AGS for room temperature operation. An atomic gold-decorated working electrode using an aqueous electrolyte, i.e., perchloric acid ($HClO_4$) is shown. Afterwards, we describe the gas measurements for a bulky amperometric sensor using a base electrolyte, i.e., potassium hydroxide (KOH). We further show the research into a miniaturized amperometric sensor by applying a room temperature ionic liquid (RTIL) to substitute for KOH, which is explained in Section 3.3.

3.3. AGSs with Room Temperature Ionic Liquids (RTILs)

To miniaturize the AGS, the system must be redesigned, i.e., the sensor dimensions including the electrolyte selection. Although the solid polymer electrolyte (SPE) has been used since the 1970s, it has a low conductivity working at room temperature and mostly is used at extreme temperatures [10]. In 1914, Paul Walden introduced the term Ionic Liquid (IL) when he reported the properties of ethyl ammonium nitrate ($[EtNH_3][NO_3]$) [31]. Ionic liquids are molten salts that are fluid over a wide range of temperatures, i.e., from low to high temperatures without any significant concentration losses due to a high thermal stability and low volatility. IL has been used for many applications, e.g., electrolyte, sensors, coating, drug delivery, enzymatic reaction, solvents, gas chromatography materials, etc. [31]. ILs can have various interactions, i.e., weak interactions, strong interactions like

the Coulombic, specific interactions, nonspecific interactions, isotropic interactions (e.g., dispersion, van der Waals forces, solvophobic forces), and anisotropic interactions (e.g., halogen bonding, dipole-dipole, magnetic dipole, electron pair donor/acceptor interactions, hydrogen bonding), etc. [44].

Room temperature ionic liquids (RTILs) are a class of ionic liquids that exist in a liquid phase below 100 °C (298 K) [11,31,44]. Recently, room temperature ionic liquid (RTIL) has been a promising choice for a miniaturized AGS operating at ambient temperature. RTIL offers many benefits: Firstly, it has negligible vapor pressure and very low volatility at room temperature thus the membrane-free gas sensor can be realized, hence, theoretically, the response time can be faster. Secondly, it is widely reported that RTIL has a wider EC potential window than liquid electrolytes which allows for detecting more target gasses where the redox reaction takes place at a high EC potential. Lastly, using RTIL, a thin film for a miniaturized AGS can be realized and the fluidity issue can be removed due to its high viscosity [27]. In this section, we also provide brief information regarding the structure and several physical-chemical properties of RTIL.

The RTIL structure is formed by the combination of a cation (positively charged) and an anion (negatively charged) [28,31]. Generally, RTIL is made from asymmetric organic cations and organic or inorganic anions [28,31]. The cation and anion combinations influence the physical and chemical properties of RTIL. For example, with regard to the melting point property, an asymmetric cation contributes to a lower melting point. As reported by MacFarlane et al., using a highly symmetrical species, ammonium and pyrrolidinium cations had a "solid" phase at ambient temperature, asymmetrical (or low-symmetry) species resulted in a "liquid" phase at ambient temperature [31,45]. The hydrophobic and hydrophilic properties of RTILs are also varied according to the cation-anion combination. Typically, the anions are responsible for water uptake. Although cations play a minor role in water absorption, the shorter the alkyl chain, the more it contributes to greater water uptake. As shown in Figure 2, the water uptake of 1-ethyl-3-methylimidazolium ($[EMIM]^+$) is greater than 1-butyl-3-methylimidazolium ($[BMIM]^+$) followed by 1-hexyl-3-methylimidazolium ($[HMIM]^+$) ≅ 1-octyl-3-methylimidazolium ($[OMIM]^+$). Figure 2 depicts the hydrophobic and hydrophilic properties of several cations and anions [6].

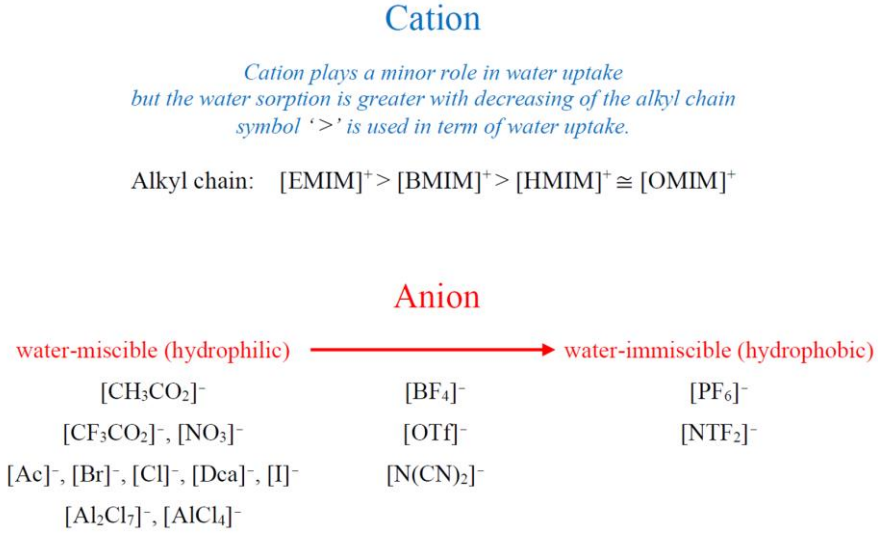

Figure 2. The water absorption from several cations and anions. Reproduced from [6].

Another important RTIL property is the electrochemical window (ECW). It is the range of the operating EC potential from the RTIL. A wider ECW allows a greater range of target gasses to be detected. The ECW is determined as the difference between anodic limit potential (V_{AL}) and the cathodic limit potential (V_{CL}) calculated in Equation (3). The cations and anions determine the V_{AL} and V_{CL}, respectively [46,47].

$$\mathrm{ECW} = V_{\mathrm{AL}} - V_{\mathrm{CL}} \quad (3)$$

Viscosity and conductivity are also important properties influenced by the combination of cation and anion. Although high viscosity can slow down the diffusion rate in EC reactions, an RTIL film with high viscosity is necessary because it must remain on the substrate. Furthermore, conductivity is the main property of the electrolyte. Since RTIL is composed of ions, i.e., cations and anions, it has purely an intrinsic conductivity that depends on the ion mobility [46,48]. In fact, the conductivity change can be associated almost directly with the viscosity change [48]. Figure 3 shows the conductivity—viscosity relation for imidazolium cation-based RTILs with different alkyl chains. As shown in Figure 3, the conductivity is decreased by the increase in alkyl chain length. A longer alkyl chain has a higher viscosity due to a high viscosity reducing the ion mobility, hence decreasing the conductivity [46]. RTIL is formed of cation-anion combinations, different pairs of cation-anion combinations; provide different physical and chemical properties.

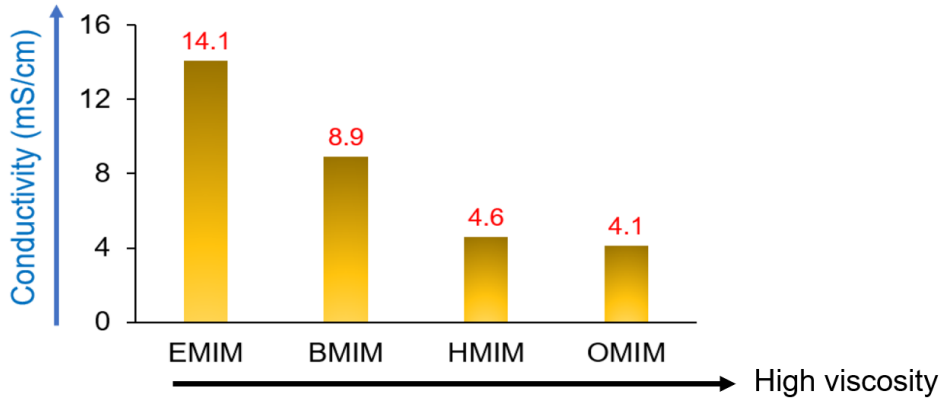

Figure 3. The relationship between conductivity and viscosity. Reproduced from [46].

In a miniaturized AGS, the amount of RTIL needed is in the microliter range or less. In 2018, Gondosiswanto et. al. used one µL of RTIL, i.e., 1-butyl-1-methylpyrrolidinium bis(trifluoromethylsulfonyl)imide ([BMP][Ntf2]), to measure oxygen gas at room temperature in a miniaturized AGS system [30]. Figure 4 shows the miniaturized AGS used two kinds of electrodes, i.e., a macro disk electrode (Figure 4a) and a microelectrode array (Figure 4b). The MDE and MEA had the same dimensional size, i.e., 10 mm × 6 mm × 0.75 mm. The MDE was made of platinum for both the CE and pseudoreference electrode, and gold material was used as the WE (diameter, 1 mm). The WE, CE, and RE of the MEA were made of gold and had a microelectrode array with 15 pairs of 10 µm electrodes. Based on the results shown in Figure 4c, the MEA had higher sensor response than the MDE (both MDE and MEA applying a fixed potential of −1.2 V). However, the work included only applying RTIL and modifying the WE without a catalyst. A catalyst is necessary to boost the performance either for bulky or miniaturized AGS systems. In Section 3.4, the information regarding several catalysts commonly used for AGS systems was provided.

3.4. AGSs with Various Catalysts

The WE is frequently doped with a catalyst to improve the sensitivity, selectivity, and the response time in the AGS system. A catalyst is a substance that increases the EC reaction rate without being consumed. A desirable catalyst should meet several criteria, i.e., it should be stable, compatible, active, selective [49]. As we know, the size of the electrode's active area influences the rate of the analyte in EC reactions. Typically, the smaller the electrode surface, the lower the sensor signal. The catalyst must be attached to the WE surface, having a long-term stability, and not dissolve in the electrolyte during the measurements. There are several catalysts commonly used in AGSs derived from metal materials and biological elements. Table 3 summarizes the various catalysts commonly applied to the WE; the benefits and drawbacks are also provided. In this research, we

focused on decorating the modified WE with atomic gold; hence, in the next section, an atomic gold catalyst is explained in more detail.

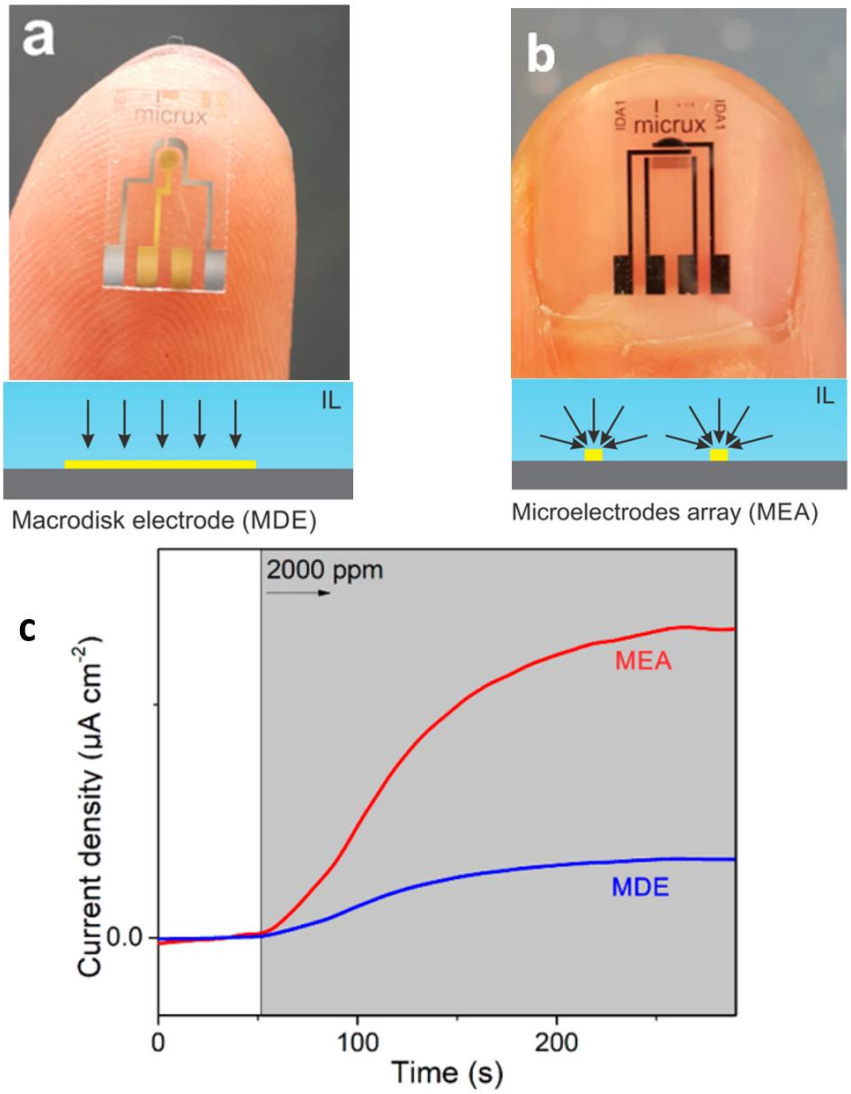

Figure 4. RTIL used in miniaturized AGS: (**a**) Macrodisk Electrode (MDE) connected to two middle terminals; (**b**) Microelectrodes Array (MEA) connected to two middle terminals; (**c**) the sensor response of MDE (blue) and MEA (red) for 2000 ppm of O_2 (black arrow shows the time when O_2 to be released). Reprinted with permission from [30]. Copyright 2018 American Chemical Society.

Table 3. Various catalysts commonly used in AGSs. Reproduced from [6].

	Catalyst	Benefits	Drawbacks	Ref.
1.	Biological element	high selectivity	short lifetime and slow response time	[7]
2.	Metal oxide (MO) nano-structures	the sensitivity can be improved by modifying the morphology; a high surface-to-volume ratio can be achieved by making a porous structure	the catalytic activity is still considered low; hence, the metal NPs are frequently added	[18,19,21,28,29]
3.	Metal nanoparticles (NPs)	high catalytic activity and sensitivity	requires a proper host matrix; the selectivity is low for isomeric compounds	[19]
4.	Atomic metal	remarkable catalytic activity, a high selectivity and sensitivity, capable of distinguishing isomeric compounds	long process; image-based validation (like SEM and TEM) has not been conducted yet due to resolution limits, particularly for atomic gold doped in PANI	[12–14,34,50]

4. Atomic Metal Catalysts

Over the past few decades, many researchers have been attracted to metal nanoparticles (NPs) with diameters less than 100 nm because their electrical, optical, chemical, magnetic, and thermodynamic properties differ from bulk metal. In other words, the catalytic activity of metal NPs are scalable corresponding to their diameter size. In contrast, metal clusters (CLs) composed of less than 100 atoms with a diameter less than 2 nm exhibit a novel catalytic property that greatly differs from those predicted by the simple scaling laws used for metal NPs. In metal clusters, the unique catalytic property is obtained due to quantum size effects and geometrical effects [15,30]. Figure 5 describes the position of metal NPs, metal clusters (CLs), and a single atom, oriented to their diameter sizes, approximate number of atoms, and molecular geometries [15,34,35].

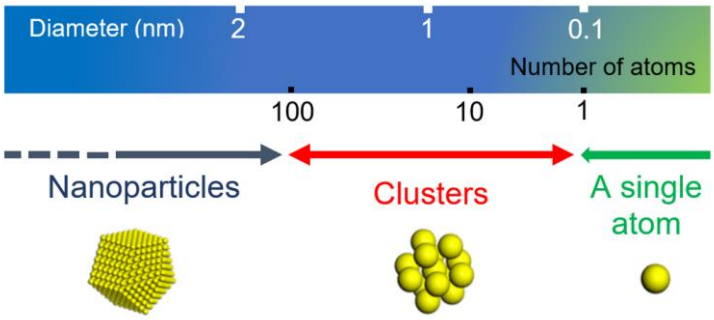

Figure 5. Illustration of metal NPs, metal CLs, and a single atom oriented to their geometry, number of atoms, and diameter size [15,34,35]. Reproduced from [6].

The catalytic activity shown by metal catalysts depends on their size, and the reduction to atomic level exhibits a remarkable catalytic property. As shown in Figure 6, although bulk metal is conductive, bulk metal (gold) is inert, resulting in a poor catalyst. When the size decreases to NPs, then the catalytic property is improved because of the increase in surface area. Furthermore, by reducing the size to atomic metal, a remarkable catalytic property is achieved due to a high density of atomic metal sited in the host matrix so that a larger active area simultaneously undergoes the catalytic activities. Figure 6 illustrates the single atom noble metal formation which started from a bulk metal to metal nanoparticles (NPs), then, down to atomic metal sited in a host matrix.

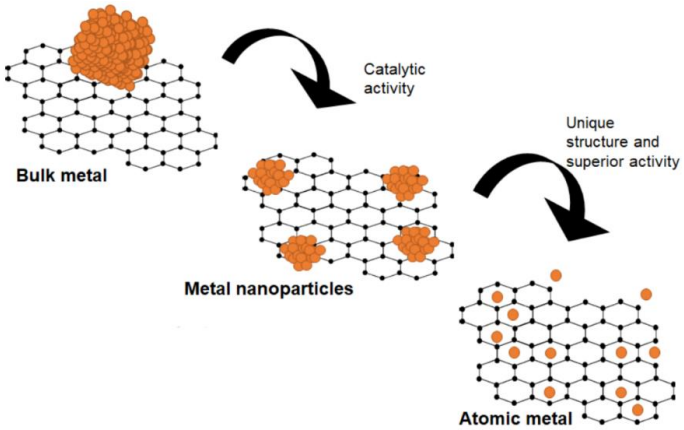

Figure 6. Illustration of atomic metal formation sited in the host matrix. The orange dot is metal. Modified from [16] with permission from John Wiley and Sons.

4.1. Polyaniline (PANI)

It is well known that a host matrix is required to site a catalyst and must be prepared first. In this research, a conducting polymer polyaniline (PANI) was selected as the host matrix. PANI was an organic conducting polymer (CP) arranged from an aniline monomer.

PANI is discovered in the mid-19th century. It is one of the oldest CPs and has been extensively studied and used in many fields due to its low cost, simple fabrication, low toxicity, biocompatibility, etc. [21,36,37]. The molecule of PANI possesses either benzenoid or quinonoid or both types [11,12,14]. Based on the reduction-oxidation state, there are three forms of PANI, i.e., leucoemeraldine state (yellow color), pernigraniline state (purple color), and emeraldine state; emeraldine base (alkaline) has a blue color and emeraldine salt (acidic) has a dark color [11,36]. Therefore, there are six forms of PANI, i.e., pernigraniline-salt, pernigraniline-base, leucoemeraldine-salt, leucoemeraldine-base, emeraldine-salt, and emeraldine-base, of which the emeraldine-salt is electronically conductive and other forms are not [11,36]. The electrical conductivity of a pure emeraldine-salt (without doping) ranges from 10^{-2} to 10^{0} S/cm [36].

The electrical conductivity of PANI can be decreased over a long cycle time [11,36]. There are several ways to diminish the drawback, i.e., doping with a catalyst, copolymerization, incorporating nanocomposites, etc. [11,36]. The doping process using PANI can be conducted in acidic media such as HCl, $HClO_4$, H_2SO_4, H_3PO_4, dodecyl-benzenesulfonic acid, camphorsulfonic acid, and para-toluenesulfonic acid, etc. [36]. Figure 7 depicts a typical cyclic voltammogram (CV) curve of PANI in an acidic solution of HCl. In acidic media, commonly, PANI has two redox peaks. The first redox occurs between 0 to 0.25 V vs. Ag/AgCl which refers to the conversion of fully reduced leucoemeraldine to partially oxidized emeraldine. Furthermore, the second redox occurs between 0.6 to 0.8 V vs. Ag/AgCl which is associated to the conversion of emeraldine to fully oxidized pernigraniline form. The EC potential of peaks 1 and 1′ corresponds to expulsion of protons and independent to the pH change, while, peaks 2 and 2′ are dependent on the pH change and responsible for the uptake of anions to the film; in addition, their shape and position strongly depend on the anion and acid type [11,36]. The irreversible degradation of PANI film occurs when a high EC potential is applied, i.e., more than 0.8 V when using acidic medium like HCl [11,36].

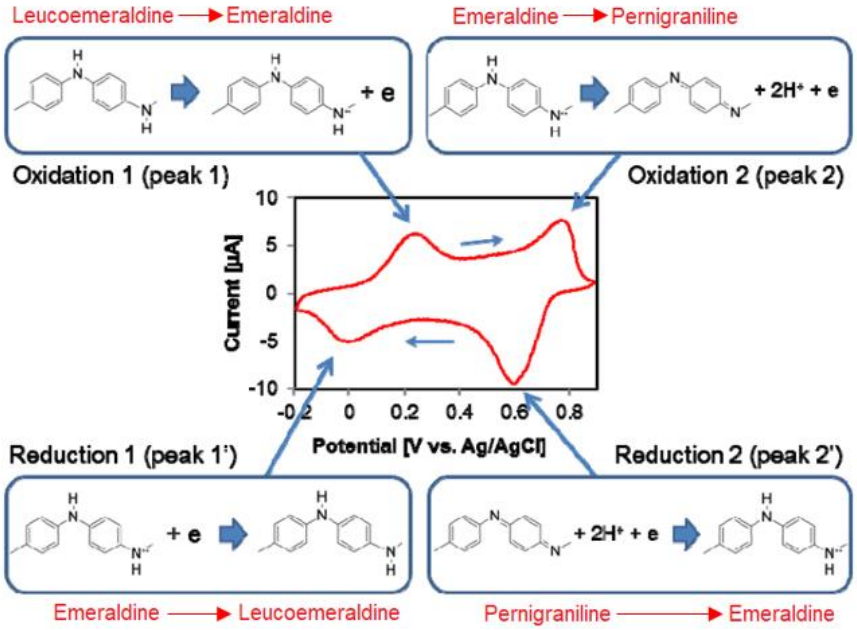

Figure 7. The common CV curve of PANI in HCl (pH = 1) shows two redox peaks coupled. Reproduced from [36].

4.2. Basic Theory of Atomic Gold Clusters

For more than four decades, due to quantum effects, the unique properties and remarkable catalytic activity possessed by atomic metal clusters (CLs) have been massively studied theoretically and experimentally [11–14,22,24]. The geometrical shape of atomic CLs is one of the main reasons for their unique properties [15]. Density functional theory (DFT), a popular tool used in many fields, has been applied for modeling quantum mechan-

ical phenomena computationally. In this field, DFT is used to determine various possible geometrical shapes that exist for atomic CLs. Figure 8 shows the various equilibrium geometrical shapes using DFT for atomic gold CLs in neutral, anionic, and cationic conditions. As depicted in Figure 8, several possible geometrical shapes exist at a certain number of clusters (n). For example, when n = 3, there are three possible geometrical shapes in which every shape possesses a unique catalytic property [51].

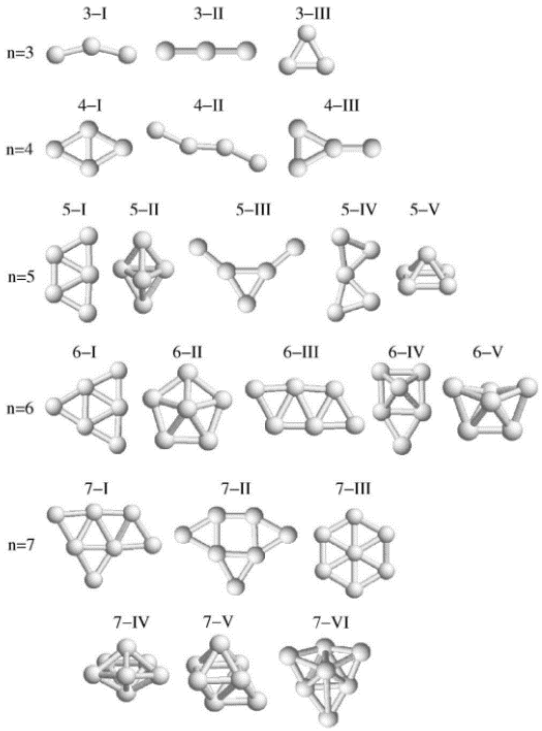

Figure 8. Various possibilities of geometrical shapes for atomic gold clusters anionic, neutral, and cationic equilibrium. The numbers of atomic gold clusters are $3 \leq n \leq 7$. Reproduced with permission from [51]. Copyright (2004) by the American Physical Society.

In the atomic metal CLs, the difference of energy between the highest occupied molecular orbital (HOMO) and the lowest unoccupied molecular orbital (LUMO), popularly known as HOMO-LUMO gap energy, is mostly utilized to confirm the atomic metal CLs formation [14,51]. DFT has been widely used to predict the HOMO-LUMO gap energy of atomic metal CLs like gold, silver, copper, etc. The formation of atomic metal CLs exhibits an odd-even pattern of HOMO-LUMO gap energy which corresponds to the number of atoms in CLs as shown in Figure 9. Typically, the HOMO-LUMO gap energy for even-numbered atomic gold clusters is higher than odd-numbered; this odd-even pattern (as depicted in Figure 9) is an indirect method to confirm the formation of atomic gold clusters. In amperometry, another way to confirm the atomic gold clusters uses the electrooxidation of full CV scans from propanol isomers in a base medium that is explained in the next section after preparation of atomic gold decorating PANI [12,14,24].

4.3. Atomic Gold Decorating PANI

Herein, the atomic gold catalyst is doped into a host matrix of PANI using an acidic medium, i.e., perchloric acid ($HClO_4$). Figure 10 depicts the process of forming the Au clusters from atom-by-atom growth in PANI. There are several procedures conducted: Firstly, sweeping the potential from −0.2 V to +0.8 V (I to II) to make fully oxidized PANI into pernigraniline form. Afterwards, the potential is held at +0.8 V (III), then, $AuCl_4^-$ anions are introduced to PANI (pernigraniline form) in situ. The PANI (pernigraniline form) uptakes one anion forming a PANI*$AuCl_4^-$ and the excess of $AuCl_4^-$ anions are rinsed away using $HClO_4$ at +0.8 V (IV). Finally, the reduction of $AuCl_4^-$ to Au (V) can be achieved

by sweeping the potential from +0.8 V to −0.2 V. Then the PANI/Au_1 (i.e., PANI doped with one atomic gold $Au_{N=1}$) is obtained. This cycle can be repeated N times to dope N atomic gold clusters in PANI, for example, PANI/Au_2 means that the atomic gold doping process is repeated twice [23,26].

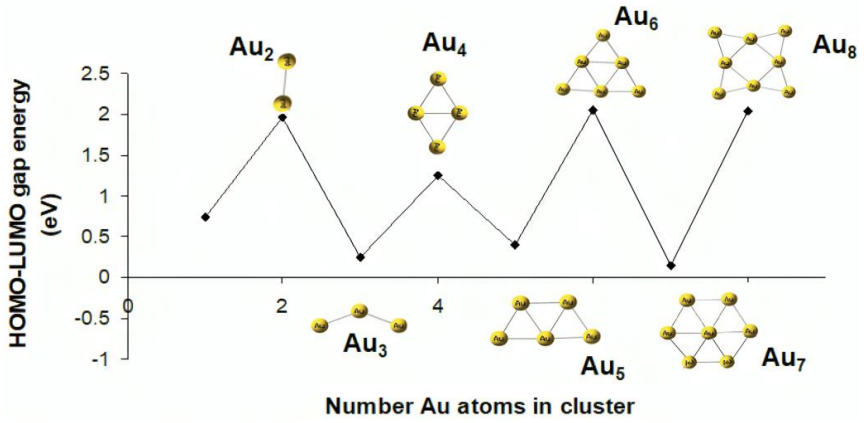

Figure 9. The predicted HOMO-LUMO gap energy for atomic gold CLs (Au_N where N = 1 to 8). Reproduced with permission from [52].

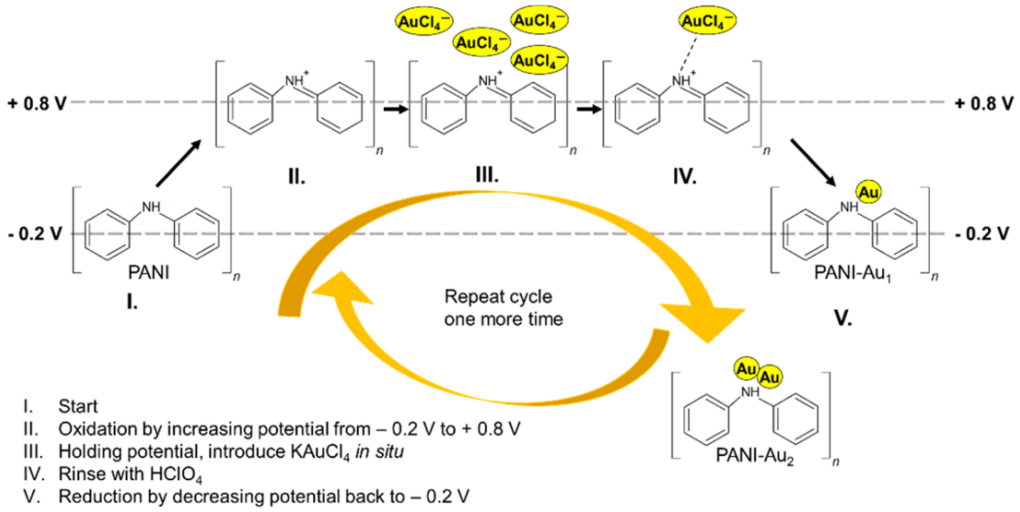

Figure 10. The procedure of doping atomic gold into host matrix of PANI using $HClO_4$. Reproduced from [26].

The full CV scans of atomic gold clusters doped in PANI using $HClO_4$ were recorded and depicted in Figure 11. The potential was swept from −0.2 V to +0.8 V vs. Ag/AgCl reference electrode forward and backward. As shown in Figure 11, CV curves of five different conditions of PANI were recorded, i.e., initial CV of PANI before doping process (I, black dash line color), the recorded CV for reduction of $AuCl_4^-$ in PANI, forming PANI/Au_1 (II, red color), the CV for PANI/Au_1 (III, blue color), the recorded CV for reduction of $AuCl_4^-$ in PANI/Au_1, forming PANI/Au_2 (IV, orange color), and the CV for PANI/Au_2 (V, green color). During the atomic gold deposition process, particularly for a higher number of atomic gold clusters, PANI is oftentimes fully oxidized for a prolonged time (+0.8 V) which frequently causes the irreversible degradation indicated by the decreased current density area. As shown in Figure 11, the current density of PANI/Au_2 was reduced (green color) compared to the initial CV of PANI (black dashed line) meaning that PANI film underwent a degradation during the doping process. Although PANI/Au_2 experienced a degradation, the performance PANI/Au_2 for propanol isomers in base medium exhibits the highest catalytic activity compared to PANI without atomic gold and PANI/Au_1. It means that the Au_2 clusters have benn successfully fabricated and sited in PANI.

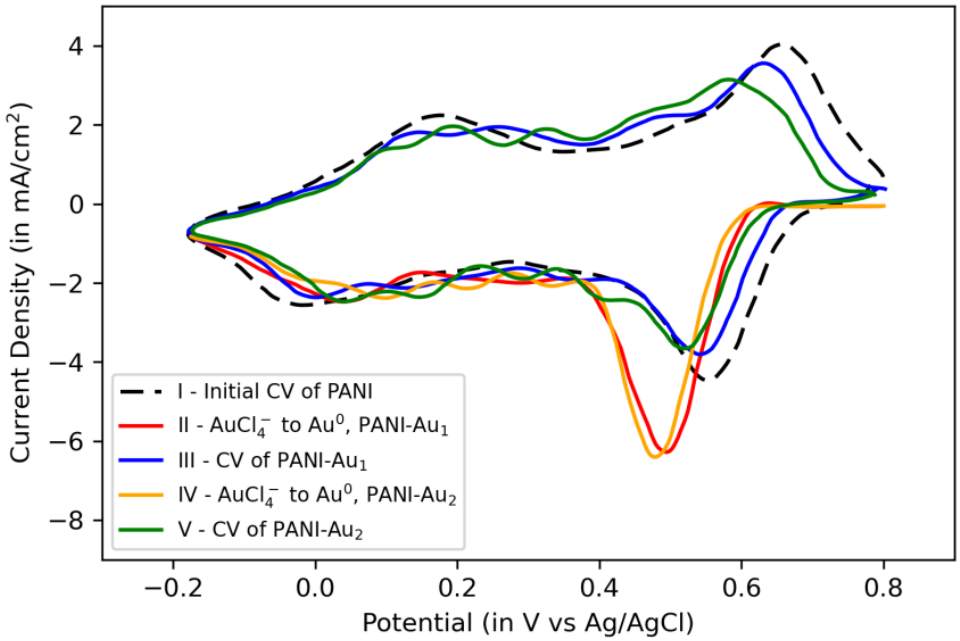

Figure 11. The CV curves of PANI in $HClO_4$ in five conditions: (I) initial PANI before deposition; (II) reduction of $AuCl_4^-$ to Au^0 in PANI (forming PANI/Au_1); (III) PANI/Au_1; (IV) reduction of $AuCl_4^-$ to Au^0 in PANI-Au_1 (forming PANI/Au_2); (V) PANI/Au_2. The scan rate = 20 mV/s. Reproduced from [24].

5. Atomic Gold-Decorated Amperometric Sensor

An atomic gold catalyst was successfully used for an amperometric sensor by Janata's research group whose works can be found here [11–14,22]. In the following years, an atomic gold deposition system in a bulky system was built in the Nakamoto Laboratory, Tokyo Tech, Tokyo, Japan [23,24]. The success of the atomic gold cluster formation in PANI was confirmed using electrooxidation of 0.5 M propanol isomers in 1 M KOH. Figure 12 depicts the effect of the number of atomic gold clusters Au_N (N = 1 to 4) in PANI for electrooxidation of propanol isomers in KOH. Several modified WEs (i.e., Pt/PANI/Au_N) were assessed in this measurement.

As shown in Figure 12a, the current densities were higher for even numbers of atomic gold clusters (N = 2 and 4) than the odd-numbered atoms (N = 1 and 3) both for 1-propanol and 2-propanol due to HOMO-LUMO gap energy variation which is similar to the obtained results from related research [12,14,53]. Two peaks occurred, i.e., peak 1 (around −0.2 V) and peak 2 (around +0.2 V). This first oxidation peak (peak 1) is associated with the platinum (Pt) electrode. The second oxidation peak (peak 2) is attributed to the presence of the atomic gold formation which gives a strong indication that atomic gold clusters sited in PANI undergo electrooxidation for propanol isomers in KOH. In addition, using Pt/PANI/Au_2, for 1-propanol, peak 1 is higher than peak 2, whereas for 2-propanol, peak 1 is lower than peak 2; these results were also similar to other related researchers' works [11–14,22].

Furthermore, as shown in Figure 12b, the odd-even pattern of peak 2 which is associated with atomic gold formation was also obtained both for 1-propanol and 2-propanol; the atomic gold clusters with even-numbered atoms showed a higher catalytic activity than the odd-numbered atoms. Thus, atomic gold cluster formation was confirmed. Later, we focused on fabricating Pt/PANI/Au_2 only for gas measurements, although the experiment here was conducted in the liquid phase.

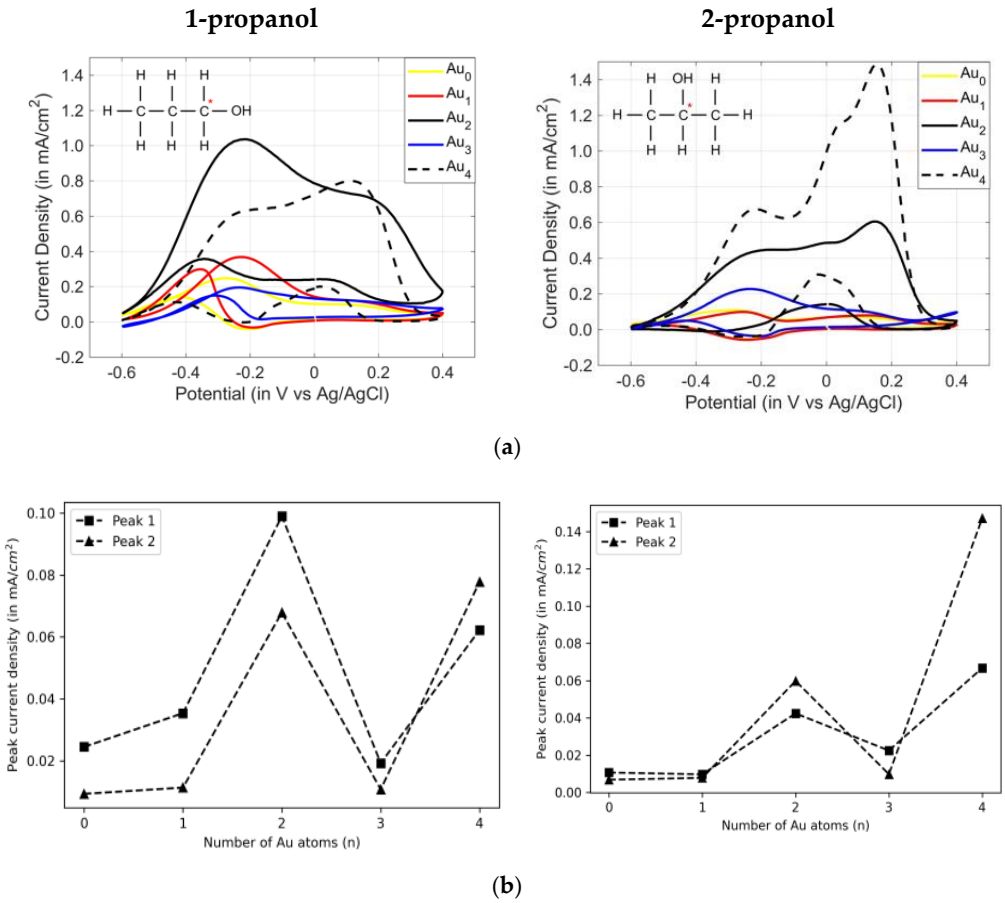

Figure 12. The electrooxidation of propanol isomers in KOH using Pt/PANI/Au_N (N = 0, 1, 2, 3 and 4): (**a**) the full CV scans; (**b**) the peak current density for peak 1 and peak 2. The scan rate was 100 mV/s. Reproduced from [23].

6. Atomic Gold Decorating a Bulky Amperometric Gas Sensor (AGS)

6.1. Atomic Gold Deposition System for a Bulky AGS

Figure 13a depicts the flow cell where the WE, CE, and RE were located. The flow cell was made from polycarbonate with diameter Ø = 60 mm fabricated by Ono denki, Japan. The WE was made of platinum (Pt) with diameter Ø = 3 mm purchased from BAS Japan. The Pt thin film (Nilaco, Tokyo, Japan) and Ag/AgCl in 3 M NaCl (BAS, Tokyo, Japan) were used as RE and CE, respectively. The flow cell had two plates, a front and a back plate. The Pt thin film as CE was sealed between a front and a back plate using a polydimethylsiloxane (PDMS) membrane and O-ring to seal the two plates to prevent electrolyte leakage.

Figure 13b shows the complete atomic gold deposition system used for a bulky AGS. The 0.2 mM potassium tetrachloroaurate ($KAuCl_4$) was dissolved in 0.1 M perchloric acid ($HClO_4$) to supply the noble metal Au. A syringe pump (Legato 110, KD Scientific, Holliston, MA, USA) was utilized to drive $KAuCl_4$ into the flow cell. Furthermore, to rinse the excess of gold anions, 0.1 M $HClO_4$ was used, and it was driven by a peristaltic pump (13-876-2, Fisher Scientific, Pittsburgh, PA, USA). A solenoid valve (EXAK-3, Takasago, Tokyo, Japan) was used to control the switching between $KAuCl_4$ and $HClO_4$. The tube used chemically inert tygon tubes (LMT-55, Saint Gobain, Courbevoie, France). The potential applied on the WE was controlled by a laboratory-fabricated potentiostat based on a low-noise JFET (Junction Field Effect Transistor) operational amplifier (TL074, Texas Instruments, Dallas, TI, USA). An Arduino was used to control the on and off states of the solenoid valve and peristaltic pump. All measurements were taken using MATLAB script file (2017a, Mathworks) via a Serial-USB protocol. The procedure for making a modified WE of

Pt/PANI/Au_1 followed the timing diagram shown in Figure 13c. Furthermore, if we want to fabricate Pt/PANI/Au_2, then the cycle, i.e., steps A to G, must be repeated twice.

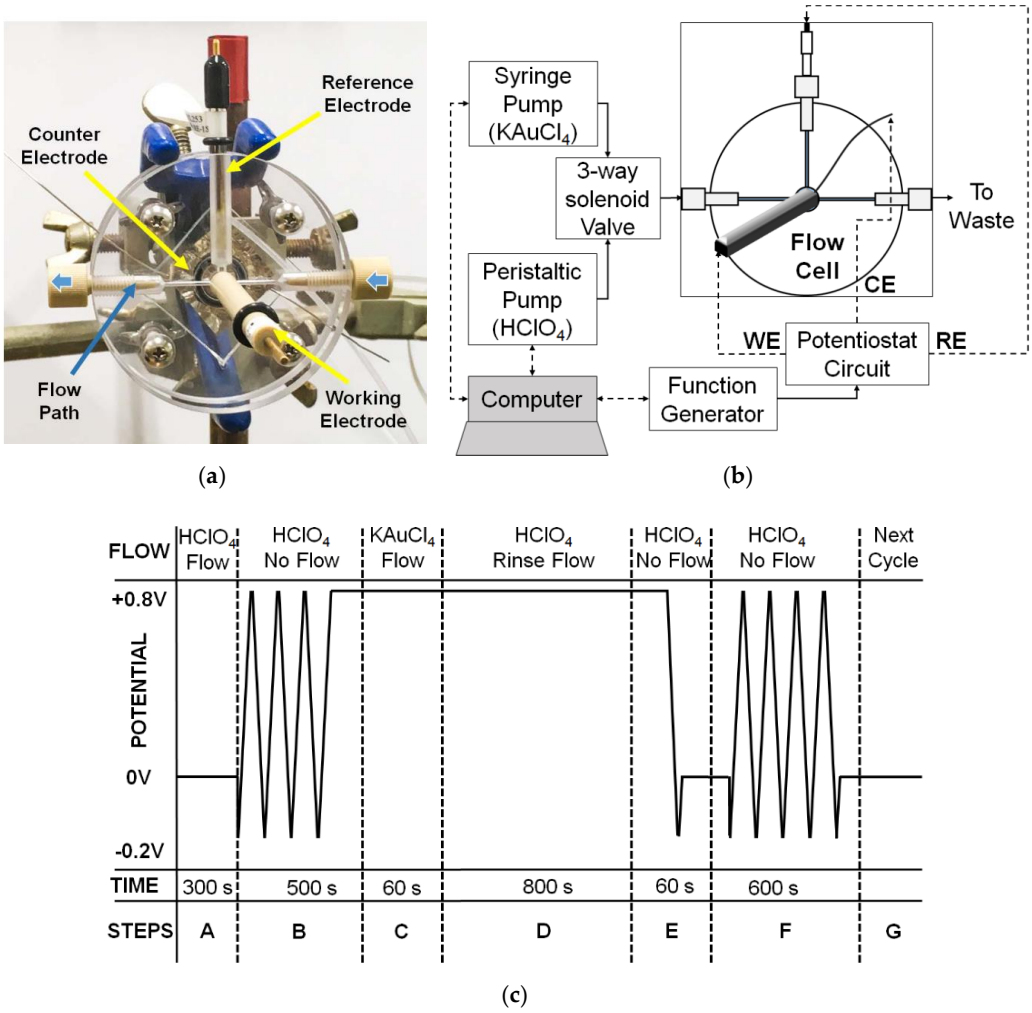

Figure 13. The atomic gold system for a bulky AGS: (**a**) the flow cell; (**b**) the complete system; (**c**) the timing diagram to fabricate PANI/Au_1. Reproduced from [23].

6.2. Sensor Fabrication and Validation

Firstly, PANI was prepared on a Pt WE (diameter Ø = 3 mm, BAS Japan) using electropolymerization of 0.1 M aniline ($C_6H_5NH_2$) in 2 M tetrafluoroboric acid (HBF_4) at a constant potential for about 200 seconds. After the atomic gold deposition process was completed, the atomic gold cluster Au_2 formation on the modified WE was checked using electrooxidation of propanol isomers in alkaline medium. Figure 14a depicts the full CV scans of Pt/PANI/Au_2 in 1 M KOH for 0.5 M 1-propanol (nPrOH) and 0.5 M 2-propanol (iPrOH), respectively. According to Figure 14a, there was a significant difference between 1-propanol and 2-propanol. Both propanol isomers had two oxidation peaks; 1-propanol (nPrOH) had a higher first peak (−0.2 V) than its second peak (+0.2 V), and 2-propanol (iPrOH) had a higher second peak (+0.2 V) than its first peak (−0.2 V), these results agreed with other related research works and the previous explanation in Section 5 (atomic gold decorating amperometric sensor) [12,14,53]. The reproducibility of Pt/PANI/Au_2 was also checked using several electrodes as shown in Figure 14b. According to Figure 14b, although some variations occurred, discriminable patterns between 1-propanol (nPrOH) and 2-propanol (iPrOH) could be seen and exhibited a similar curve to that in Figure 14a.

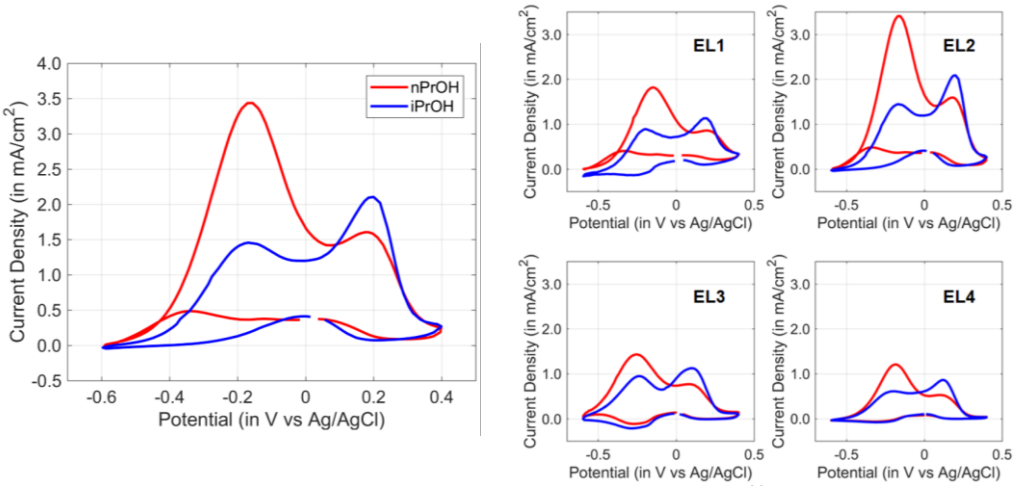

(**a**) (**b**)

Figure 14. The electrooxidation of 0.5 M propanol isomers in 1 M KOH using Pt/PANI/Au_2: (**a**) the full CV scans; (**b**) the reproducibility of several electrodes. The scan rate was 100 mV/s. Reproduced from [23].

6.3. Response to Propanol Isomers in Gaseous Phase

The atomic gold-decorated amperometric sensor with the analytes in liquid phase has been massively studied and reported by Janata's and other related research [11–14,22]. Chakraborty et al., progressed this research for a gaseous phase measurement. Herein, we provided the gaseous phase measurement for propanol isomers using the system shown in Figure 15. The propanol vapor was exposed to the bulky AGS system (WE: Pt/PANI/Au_2) for 5 min and the CV curve was recorded. Figure 15a,b depict the CV response for nPrOH and iPrOH, respectively. CV curves with several concentrations are included, i.e., 0%, 30%, 60% and 90% of full-scale concentration of 1600 ppm (measured using ppbRAE 3000, RAE Systems, Schaumburg, IL, USA). Based on Figure 15a,b, there was a clear difference between the curves for a concentration of 0% (without analytes) and the presence of the analytes. For gaseous nPrOH, the peak at −0.2 V was more discriminable, moreover, for 90% concentration. For iPrOH, using concentrations of 30% and 60%, both the oxidation peaks at − 0.2 V and +0.2 V have strongly discriminable features; when using 90% concentration, the peak at − 0.2 V is lower than the peak at +0.2 V. Based on these results, the measurement of propanol isomers in the gaseous phase was similar to those in the liquid phase meaning that Pt/PANI/Au_2 was catalytically active for gas measurements.

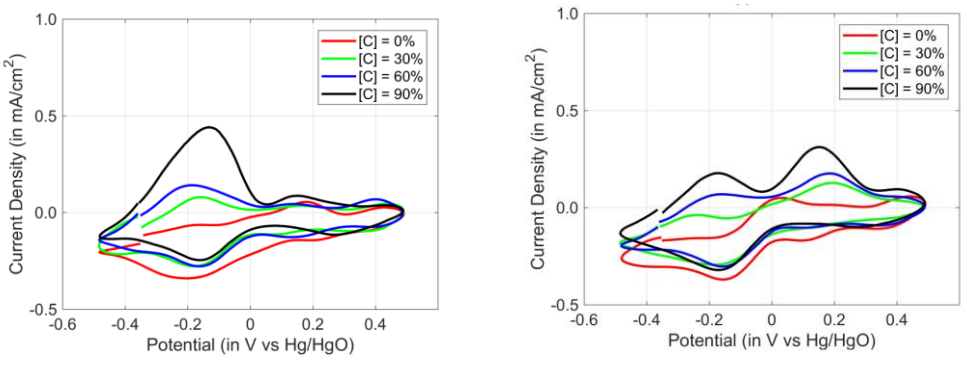

(**a**) (**b**)

Figure 15. Gaseous propanol isomer measurement using Pt/PANI/Au_2 at various concentrations ([C] = % concentration of full scale 1600 ppm): (**a**) the CV scans of 1-propanol; (**b**) the CV scans of 2-propanol. The scan rate was 100 mV/s. Reproduced from [23].

These works successfully demonstrated the formation of atomic gold in a bulky AGS system. In addition, Pt/PANI/Au_2 exhibited electrocatalytic activity even in gas measurements. Afterward, we developed this research into a miniaturized AGS system as shown in Figure 16. The sensor design, electrolyte, and atomic gold deposition system will be redesigned and explained in more detail in Section 7.

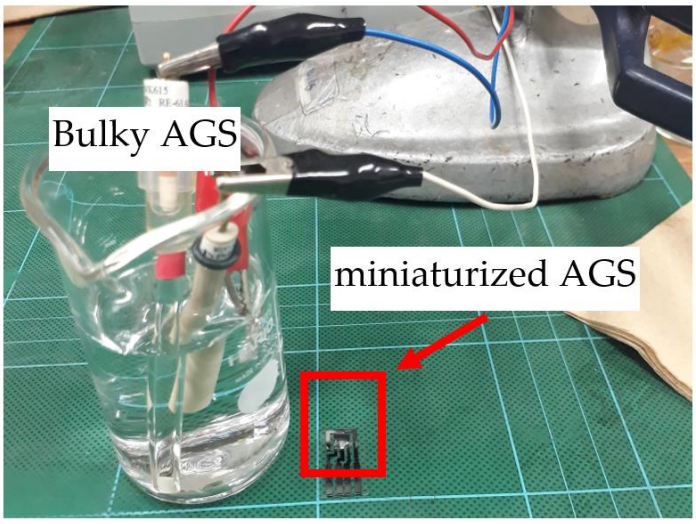

Figure 16. Conversion from a bulky AGS to a miniaturized AGS.

7. Atomic Gold Decorated Miniaturized Amperometric Gas Sensor (AGS)

7.1. A Miniaturized Amperometric Gas Sensor (AGS)

An interdigitated array electrode (IDA) as shown in Figure 17 was selected for the miniaturized AGS in which all the electrodes made from platinum and deposited on a same quartz plate (glass) substrate. The commercial IDA was purchased from BAS Co., Ltd., Tokyo, Japan. The detailed IDA structure is depicted in Figure 17.

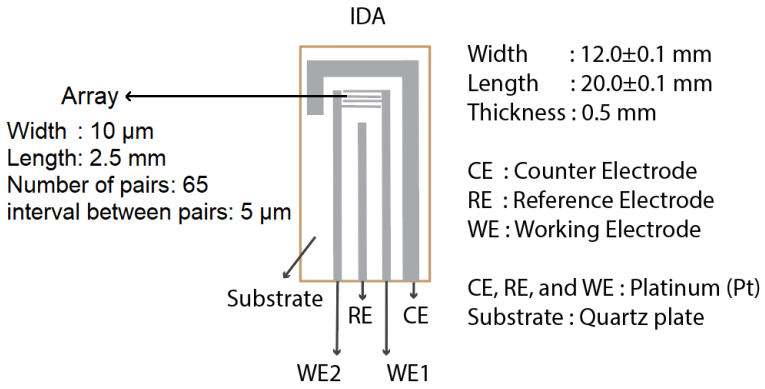

Figure 17. The interdigitated array (IDA) electrode selected for a miniaturized AGS. Reproduced from [27].

7.2. RTILs as Electrolytes

In the miniaturized AGS, besides redesigned sensor dimensions, the electrolyte was also changed. Herein, the RTIL was selected to substitute for the volatile aqueous electrolyte (e.g., KOH). The common RTIL imidazolium was chosen and used without further purification (purchased from Tokyo Chemical Industry Ltd., Tokyo, Japan). Three RTILs having the same cations and different anions were used, i.e., 1-ethyl-3-methylimidazolium acetate ([EMIM][Ac]), 1-ethyl-3-methylimidazolium trifluoromethanesulfonate ([EMIM][Otf]), and 1-ethyl-3-methylimidazolium chloride ([EMIM][Cl]). The different pairs of cation-anion combinations possess different physical and chemical properties summarized in Table 4.

Table 4. The basic physicochemical properties of the RTILs used. Reproduced from [27].

Identifier	CAS Number	Full Name	Viscosity, η (P a s)	Density, ρ (Kg/m^3)	Conductivity, κ (S/m)	EC Window (V)
[EMIM] [Ac]	143314-17-4	1-ethyl-3-methylimidazolium acetate	0.143	1099.3	0.2	−2.3 to +0.9
[EMIM] [Otf]	145022-44-2	1-ethyl-3-methylimidazolium trifluoromethane-sulfonate	0.042	1385.9	0.9	4.3
[EMIM] [Cl]	65039-09-0	1-ethyl-3-methylimidazolium chloride	0.047 (a)	1112 (a)	0.108	-

The information of η, ρ, and κ at 298 K (25 °C), except (a) 353.15 K (80 °C).

7.3. Atomic Gold Deposition System for the Miniaturized AGS System

Figure 18a depicts the chamber for installing IDA electrode used for atomic gold deposition process. The IDA was installed using USB connector to the chamber. The USB socket has four pins for the IDA's electrode lines, i.e., WE 1, WE 2, RE, and CE. During the deposition process, the CE and WEs from IDA and the external RE of Ag/AgCl were connected to a lab-fabricated potentiostat (based on IC TL074, Texas Instruments, Dallas, TX, USA). Figure 18b shows the complete atomic gold deposition system for a miniaturized AGS. The working principle of atomic gold deposition process and timing diagram for a miniaturized AGS was the same as the atomic gold for a bulky AGS system explained in Section 6.1; However, the flow cell was changed to a chamber as shown in Figure 18.

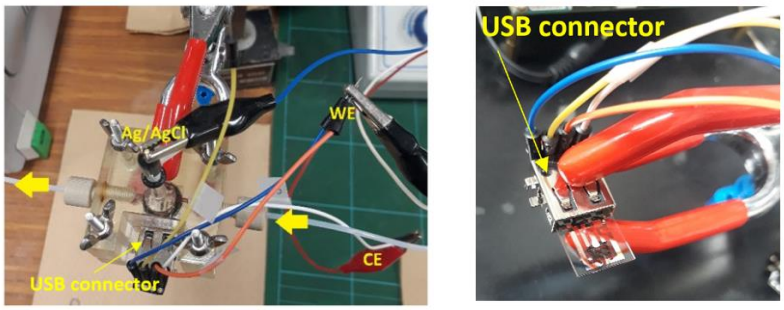

(**a**) (**b**)

Figure 18. The atomic gold deposition system: (**a**) the chamber for the IDA electrode; (**b**) the schematic of the complete system. Reproduced from [27].

7.4. Sensor Fabrication and Validation

The WEs were polymerized with polyaniline. The polymerization of PANI was conducted in Sone Laboratory at Tokyo Institute of Technology, Tokyo, Japan. The PANI was used as a support matrix, polymerized using 0.1 M aniline ($C_6H_5NH_2$) in 2 M tetrafluoroboric acid (HBF_4). The electropolymerization of PANI used the Galvanostatic method with a constant current of 0.56 mA for 260 s. The thickness was approximately 0.05 mm. Figure 19 depicts the CV curve of modified IDA electrodes in the 0.1 M $HClO_4$, i.e., Pt/PANI/Au_0 (black color), Pt/PANI/Au_1 (red dashed line), and Pt/PANI/Au_2 (blue line). As shown in Figure 19, the current density of Pt/PANI/Au_2 experienced a reduction which also occurred in the bulky system. This degradation is due to the PANI film being held at high potential (at +0.8 V) for a long time during the atomic gold deposition process.

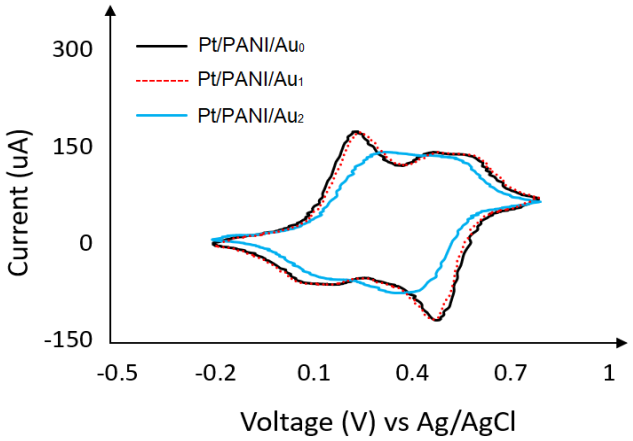

Figure 19. The CV curve of several modified IDA electrodes in 0.1 M $HClO_4$. The scan rate was 50 mV/s. Reproduced from [6].

Figure 20 show the measurement results of electrooxidation from 0.5 M propanol isomers in 1 M KOH using three different modified IDA electrodes, i.e., Pt/PANI/Au_0 (without atomic gold, black dashed line), Pt/PANI/Au_1 (red dashed line), and Pt/PANI/Au_2 (blue for 1-propanol and green for 2-propanol). As shown in Figure 20, Pt/PANI/Au_2 had the highest current density compared to Pt/PANI/Au_0 and Pt/PANI/Au_1. The obtained electrooxidation results for 1-propanol and 2-propanol were also like the Pt/PANI/Au_2 in a bulky system, i.e., 1-propanol had a higher first peak (at −0.2 V) than its second peak (+0.2 V), 2-propanol had a higher second peak (at +0.2 V) than its first peak (at −0.2 V). Thus, we confirmed the success of Au_2 cluster formation on the miniaturized AGS.

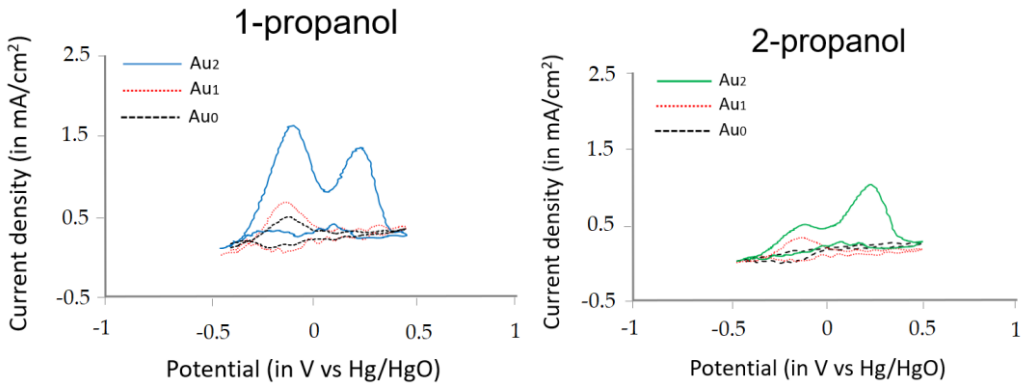

Figure 20. The electrooxidation of 1-propanol and 2-propanol using a miniaturized AGS. The scan rate was 50 mV/s. Reproduced from [27].

7.5. Sensors Using RTIL to Develop a Miniaturized AGS

In this research work, we also incorporated a microgravimetric sensor, i.e., a quartz crystal microbalance sensor (QCM) to check the possibility of target gas adsorption in RTIL. QCM is a very mass-sensitive sensor and has a high stability. QCM follows the Sauerbrey formula where the frequency change is proportional to the amount of adsorbed mass (from analyte) on its surface [39,54,55]. Three AT-CUT QCMs, having a basic resonant frequency of 9 MHz, were used (purchased from Seiko EG&G Ltd., Tokyo, Japan). The three RTILs used for the IDA were also used as coating on QCMs, i.e., [EMIM][Ac], [EMIM][Otf], and [EMIM][Cl]. The dip-coating method was used to coat the RTIL onto the QCM as illustrated in Figure 21 (dip coater: VLAST45-06-0100, THK Co., Ltd., Tokyo, Japan). Furthermore, the coating information for the QCM is provided in Table 5.

Before conducting gas measurement, the platinum RE of the IDA electrode must be painted using Ag/AgCl ink (purchased from BAS Co., Ltd., Tokyo, Japan). A RE using Ag/AgCl is preferable to avoid a voltage drop and to maintain a stable EC reaction [54].

Figure 22a shows the painting of Ag/AgCl ink to cover the platinum RE. The Ag/AgCl ink was allowed to dry for around 2 days to obtain strong adhesion to the platinum RE. Both Pt/PANI/Au_0 and Pt/PANI/Au_2 electrodes had a dried Ag/AgCl ink applied to their RE. Afterward, 5 µL of RTIL was drop-casted on the IDA electrode surface as shown in Figure 22b, where all the WEs, CE, and RE were covered. Furthermore, the estimated thickness of RTILs drop-casted on the IDA was measured using the QCM, as summarized in Table 6.

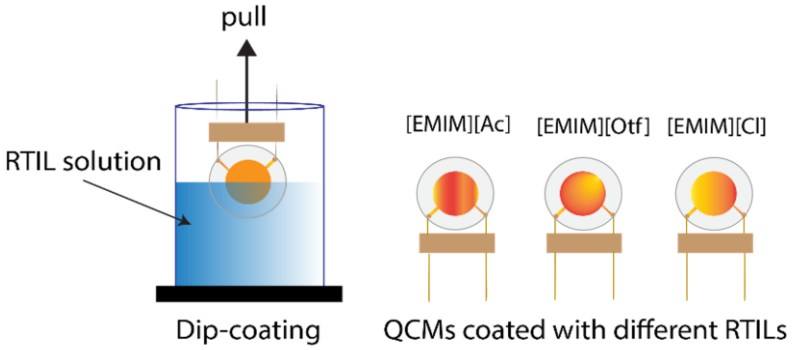

Figure 21. Three different RTILs coated on QCM using dip-coating method. Reproduced from [27].

Table 5. The coating information for the QCM. Reprinted from [27].

Identifier	QCM Coating Information					
	Solvent	**Concentration (mg/mL)**	**Pull-Up Speed (µm/s)**	**ΔF (Hz)**	**ΔM (µg)**	***d*** **(nm)**
[EMIM][Ac]	Acetone	10	1000	435	0.46	17.12
[EMIM][Otf]	Acetone	9.09	1000	577	0.62	28.50
[EMIM][Cl]	Acetonitrile	9.09	100	872	0.93	33.09

ΔF is the frequency change, d is the coating thickness, assumed to be distributed uniformly on gold electrodes on the QCM's plate, and ΔM is the mass loaded after the dip-coating process calculated from Sauerbrey's equation [54].

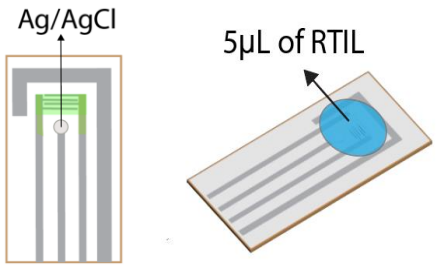

(**a**) (**b**)

Figure 22. The preparation before gas measurements: (**a**) Ag/AgCl ink painted and dried on RE; (**b**) 5 µL of RTIL drop-casted on IDA surface. Reproduced from [27].

Table 6. The thickness of RTILs drop-casted on the IDA estimated using QCM. Reproduced from [6].

Identifier	QCM's Coating Information			
	ΔF (Hz)	**ΔR (Ω)**	**ΔM (µg)**	***d*** **(nm)**
[EMIM][Ac]	5206.089	883.77	5.5	516.91
[EMIM][Otf]	5921.939	945.09	6.3	467.36
[EMIM][Cl]	2186.273	871.9	2.3	215.05

The RTIL thickness was assumed to be distributed uniformly on one side of the QCM's electrodes. The mass loaded was calculated from Sauerbrey's formula [54].

7.6. Response to Butanol Isomers in Gaseous Phase

This work also incorporated a microgravimetric sensor working simultaneously with the IDA during the gas measurement. QCMs coated with the same RTILs as used for the IDA were used to check the solubility of the target gas compound in the RTILs and to provide a broad understanding related to the sensing behavior of RTILs with different transducers. Different relative concentrations of butanol isomers were explored, i.e., 0%, 25%, 50%, 75%, and 100%; relative concentration was the relative concentration to the full scale of the ODS system with 6 mL of analyte put in the vial measured by a photoionization sensor (RAE 3000 PID). The amount of concentration released by ODS and its equivalent to RAE 3000 PID (in ppm) reading is available in Figure 23. As shown in Figure 23, using QCM coated with the same RTILs used for the IDA, the solubility of *1*-butanol vapors was recorded which showed by frequency change response even for low 25% concentration. As shown in Figure 23, QCMs coated with RTILs exhibited the same trends, i.e., the higher the concentration of target gas, the higher the frequency change response. QCM follows Sauerbrey's formula, i.e., the loaded mass on its surface is proportional to frequency change and different frequency change magnitudes are due to varying adsorptions of each RTIL to the certain target gas concentration. Furthermore, for the miniaturized AGS, as shown in Figure 24, Pt/PANI/Au_2 exhibited a higher current density than Pt/PANI/Au_0 meaning that atomic gold clusters of Au_2 were catalytically active in RTIL of [EMIM][Ac].

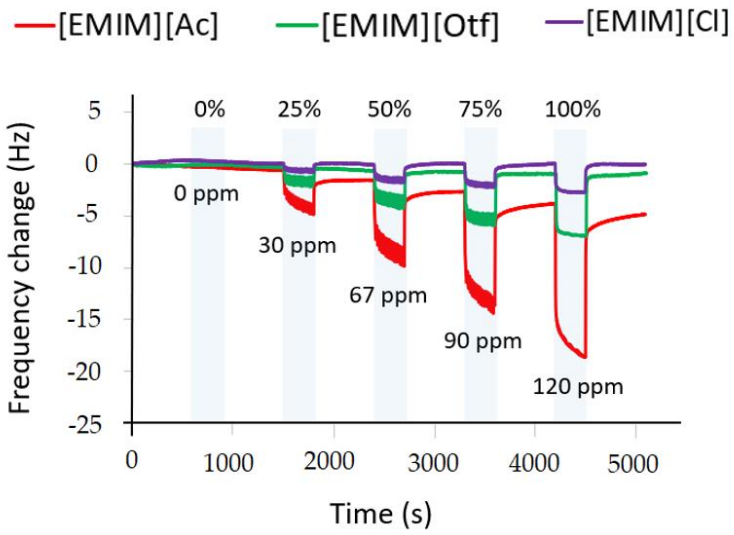

Figure 23. Various concentrations of gaseous 1-butanol were explored to check the solubility of target gas using QCM coated with RTIL. Each experiment had 5 min for target gas exposure and 10 min for recovery (N_2 flow). Reproduced from [27].

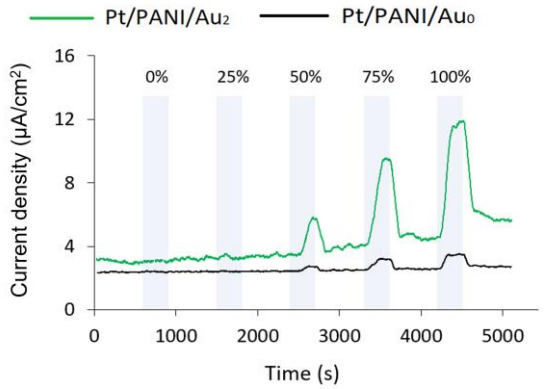

Figure 24. 1-butanol vapor measurement using miniaturized AGS. Reproduced from [27].

Figure 25 shows the sensor response from Pt/PANI/Au_2 and Pt/PANI/Au_0 for butanol isomers at 100% RC with five repeated measurements per analyte. Various EC potentials for each RTIL were explored. The results for [EMIM][Ac], [EMIM][Otf], [EMIM][Cl] are shown in Figure 25a–c, respectively. As depicted in Figure 25a, using [EMIM][Ac], three fixed potentials were used for the measurement of butanol isomers, i.e., +0.25 V, +0.5 V, and +0.9 V against the Ag/AgCl reference electrode. According to Figure 25a, Pt/PANI/Au_2 contributed more to the measurement of butanol isomers vapors because it showed a higher sensor response than Pt/PANI/Au_0. Furthermore, for [EMIM][Otf] shown in Figure 25b, Pt/PANI/Au_2 was the only electrode contributing to the measurement of gaseous butanol isomers, whereas Pt/PANI/Au_0 had no response. Lastly, for [EMIM][Cl] as shown in Figure 25c, the influence of Pt/PANI/Au_2 was not significant compared to Pt/PANI/Au_0. Overall, Pt/PANI/Au_2 showed a particular electrocatalytic activity depending on the RTIL and fixed potential.

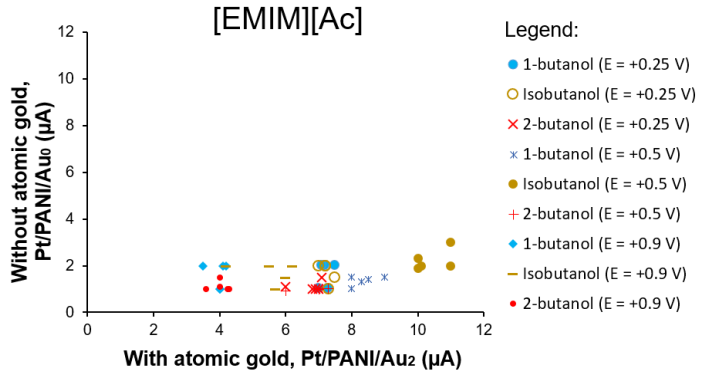

(**a**)

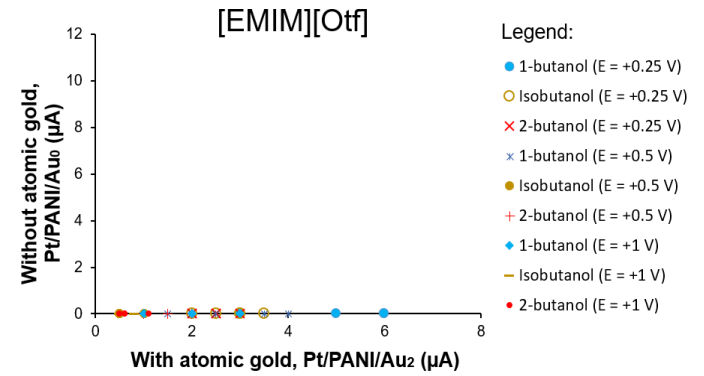

(**b**)

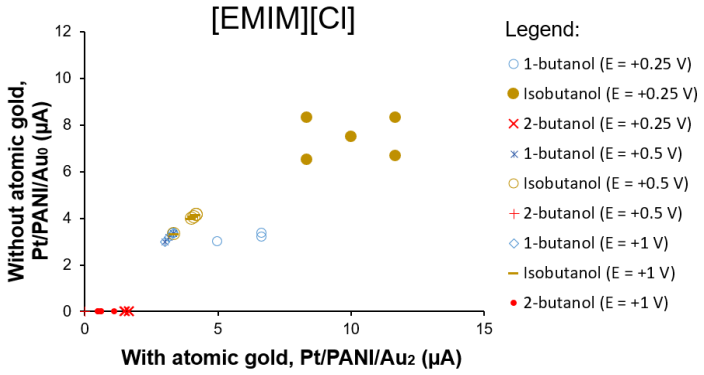

(**c**)

Figure 25. The sensor response from Pt/PANI/Au_2 and Pt/PANI/Au_0 from five measurements at 100% RC of butanol isomers for: (**a**) [EMIM][Ac]; (**b**) [EMIM][Otf]; (**c**) [EMIM][Cl]. Reproduced from [6].

Figure 26 shows the comparative results of several miniaturized AGSs using [EMIM][Ac], i.e., Pt only, Pt/PANI/Au_0, and Pt/PANI/Au_2. Figure 26 depicts average sensor responses from five measurements. An amount of 5 µL of [EMIM][Ac] was used as the electrolyte and dried Ag/AgCl ink as the RE. The butanol isomer vapors were at 100% concentration. The analyte's exposure time was 5 min, followed by 10 min (N_2 flows) of recovery time. According to Figure 26, Pt/PANI/Au_2 exhibited the highest sensor response for all butanol isomers vapors at all fixed potentials, i.e., +0.25 V, +0.5 V, +0.9 V, meaning that the electrocatalytic properties possessed by the Au_2 clusters influenced the enhanced sensitivity of gaseous butanol isomers compared to Pt/PANI/Au_0 and the commercial Pt IDA electrode.

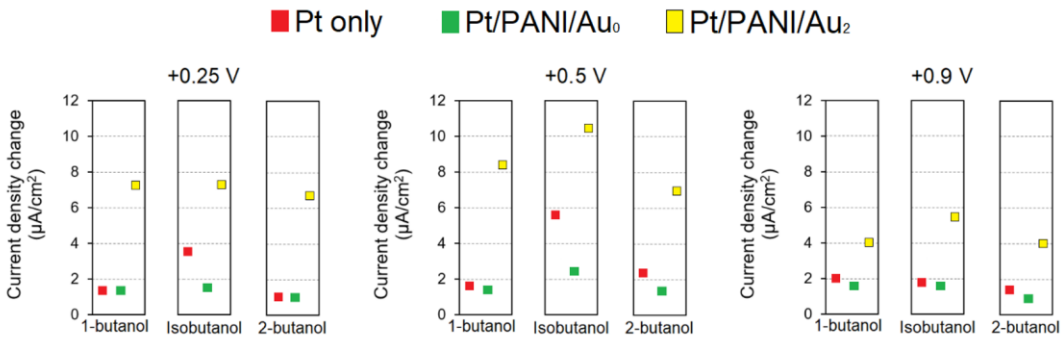

Figure 26. The sensor response for several AGSs coated with [EMIM][Ac] at fixed potentials of +0.25 V, +0.5 V, and +0.9 V vs. Ag/AgCl. Reproduced from [27].

8. Performance Enhancement of Miniaturized AGSs in the Future

In this review paper, we put our perspectives enhancing the performance of miniaturized AGSs in the future. So far, a miniaturized AGS with RTIL has not been released onto the commercial market. In this work, we successfully verified and demonstrated the enhanced sensor response to the measurement of butanol isomers using atomic gold on a miniaturized AGS with different RTILs. However, the sensor response was not enhanced significantly compared to those IDA electrodes without atomic gold. The sensitivity was not as high as in an alkaline medium when using a bulky AGS system. The current challenges and improvements can be explained as follows:

1. A slow diffusion transport. It is widely reported that RTIL has a high viscosity thus leading to a slower diffusion transport than aqueous electrolytes like KOH, NaOH, etc. Therefore, a thin RTIL sensing film could enhance both responses and sensitivity compared to a thick RTIL film [25,26];
2. The electrode. The miniaturized AGS electrode must be redesigned to use a thin layer of RTIL. According to C.A. Gunawan et.al. and R. Gondosiswanto et.al. [25,26], a micro-electrode array type offered a higher sensitivity than the macro-electrode because it could form a thinner RTIL although it had a smaller area. There are several ways to make a micro-electrode array, for example by using partial printing in which a hydrophobic layer of 1-hexadecanethiol (HDT) was used to set a boundary between fingers. The boundary is important to keep a thin RTIL since the aggregation of RTILs between neighbours often occurs, forming a thick RTIL;
3. The density of atomic gold. As the WE area gets shrinkage in a miniaturized AGS, a high density of atomic gold is preferrable to achieve a high catalytic activity. To increase the density of atomic gold, a porous host matrix is preferrable. It is widely reported that using a porous PANI the atomic metal can be doped not only on the surface but also inside the PANI, and thus it can boost the catalytic activity [56,57]. In addition, a study regarding optimization of the atomic gold deposition process must be conducted, such as the flow rate and the concentration of the solution.

In future trends, a miniaturized sensor is favorable because it possesses many advantages, such as easy chip integration, lower concentration of target compound detection, rapid response, etc. [1–4]. However, a major issue is the low signal response. Atomic gold

catalyst doping in AGSs shows promising results by achieving a higher sensor response than AGSs without atomic gold. Therefore, an atomic metal catalyst with RTIL films is a new frontier in miniaturized AGS systems. Several ways have been explained to improve the performance. If we achieve all things above, a sensor with a high selectivity, sensitivity, and fast response time can be realized. In addition, since there are many RTILs available on the market, a gas sensor array system can be realized. AGS array technology has been massively used for chemical detection of gases which is also well known as the electronic nose [58–60].

Author Contributions: Conceptualization, T.N.; methodology, T.N., P.C. and A.F.; software, A.F. and P.C.; validation, A.F., T.N., P.C., T.-F.M.C. and M.S.; formal analysis, A.F. and T.N.; investigation, A.F.; resources, T.N., T.-F.M.C. and M.S.; data curation, A.F.; writing—original draft preparation, A.F.; writing—review and editing, T.N., P.C., T.-F.M.C. and M.S.; visualization, A.F.; supervision, T.N., P.C., T.-F.M.C. and M.S.; project administration, T.N.; funding acquisition, T.N. All authors have read and agreed to the published version of the manuscript.

Funding: This research received no external funding.

Institutional Review Board Statement: Not applicable.

Informed Consent Statement: Not applicable.

Data Availability Statement: The data presented in this study are available on request from the corresponding author.

Acknowledgments: We wish to thank Jiri Janata and Mira Josowicz of Georgia Tech for their helpful advice.

Conflicts of Interest: The authors declare no conflicts of interest.

References

1. Gas Sensor Market—By Product (Oxygen (O_2)/Lambda Sensors, Carbon Dioxide (CO_2) Sensors, Carbon Monoxide (CO) Sensors, NOx Sensors), By Technology (Electrochemical, Semiconductor, Solid State, PID, Catalytic, Infrared), By Connectivity, By Application & Forecast, 2023–2032. Available online: https://www.gminsights.com/industry-analysis/gas-sensors-market-size (accessed on 20 February 2023).
2. Gas Sensors Market. Available online: https://www.marketsandmarkets.com/Market-Reports/gas-sensor-market-245141093.html (accessed on 20 February 2023).
3. Gas Sensor Market, Global Industry Analysis, Size, Share, Growth, Trends, Regional Outlook, and Forecast 2023–2030. Available online: https://www.precedenceresearch.com/gas-sensor-market (accessed on 20 February 2023).
4. Gas Sensor Market Size, Share & Trends Analysis Report by Product (Oxygen/Lambda Sensors, Carbon Dioxide Sensors), by Type (Wired, Wireless), by Technology, by End-Use, by Region, and Segment Forecasts, 2023–2030. Available online: https://www.grandviewresearch.com/industry-analysis/gas-sensors-market (accessed on 20 February 2023).
5. Viciano-Tudela, S.; Sendra, S.; Parra, L.; Jimenez, J.M.; Lloret, J. Proposal of a Gas Sensor-Based Device for Detecting Adulteration in Essential Oil of Cistus Ladanifer. *Sustainability* **2023**, *15*, 3357. [CrossRef]
6. Faricha, A. Miniaturized Amperometric Gas Sensor with Atomic Gold Decorated Polyaniline/Platinum Composites in Room Temperature Ionic Liquid Film. Ph.D. Thesis, Department of Information and Communications Engineering, Tokyo Institute of Technology, Tokyo, Japan, 2023.
7. Kuretake, T.; Kawahara, S.; Motooka, M.; Uno, S. An Electrochemical Gas Biosensor Based on Enzymes Immobilized on Chromatography Paper for Ethanol Vapor Detection. *Sensors* **2017**, *17*, 281. [CrossRef]
8. Wei-Hao Li, M.; Ghosh, A.; Venkatasubramanian, A.; Sharma, R.; Huang, X.; Fan, X. High-Sensitivity Micro-Gas Chromatograph-Photoionization Detector for Trace Vapor Detection. *ACS Sens.* **2021**, *6*, 2348–2355. [CrossRef]
9. Zimmer, C.M.; Kallis, K.T.; Giebel, F.J. Micro-Structured Electron Accelerator for the Mobile Gas Ionization Sensor Technology. *J. Sens. Sens. Syst.* **2015**, *4*, 151–157. [CrossRef]
10. Stetter, J.R.; Li, J. Amperometric Gas Sensors—A Review. *Chem. Rev.* **2008**, *108*, 352–366. [CrossRef]
11. Saheb, A.H. Sensing Materials Based on Ionic Liquids. Ph.D. Thesis, Georgia Institute of Technology, Atlanta, GA, USA, 30 June 2008.
12. Jonke, A.P.; Josowicz, M.; Janata, J. Polyaniline Doped with Atomic Gold. *J. Electrochem. Soc.* **2011**, *158*, E147. [CrossRef]
13. Jonke, A.P.; Josowicz, M.; Janata, J. Polyaniline Electrodes Containing Tri-Atomic Au/Pd Clusters: Effect of Ordering. *Catal. Letters* **2013**, *143*, 1261–1265. [CrossRef]
14. Jonke, A.P.; Josowicz, M.; Janata, J. Odd-Even Pattern Observed in Polyaniline/(Au 0–Au 8) Composites. *J. Electrochem. Soc.* **2012**, *159*, P40–P43. [CrossRef]

15. Tsukuda, T. Toward an Atomic-Level Understanding of Size-Specific Properties of Protected and Stabilized Gold Clusters. *Bull. Chem. Soc. Jpn.* **2012**, *85*, 151–168. [CrossRef]
16. Bayatsarmadi, B.; Zheng, Y.; Vasileff, A.; Qiao, S.Z. Recent Advances in Atomic Metal Doping of Carbon-Based Nanomaterials for Energy Conversion. *Small* **2017**, *13*, 1–19. [CrossRef] [PubMed]
17. Korotcenkov, G.; Brinzari, V.; Cho, B.K. Conductometric Gas Sensors Based on Metal Oxides Modified with Gold Nanoparticles: A Review. *Microchim. Acta* **2016**, *183*, 1033–1054. [CrossRef]
18. Sun, Y.F.; Liu, S.B.; Meng, F.L.; Liu, J.Y.; Jin, Z.; Kong, L.T.; Liu, J.H. Metal Oxide Nanostructures and Their Gas Sensing Properties: A Review. *Sensors* **2012**, *12*, 2610–2631. [CrossRef] [PubMed]
19. Zhu, L.Y.; Ou, L.X.; Mao, L.W.; Wu, X.Y.; Liu, Y.P.; Lu, H.L. *Advances in Noble Metal-Decorated Metal Oxide Nanomaterials for Chemiresistive Gas Sensors: Overview*; Springer Nature: Singapore, 2023; Volume 15, ISBN 0123456789.
20. Liu, L.; Wang, Y.; Liu, Y.; Wang, S.; Li, T.; Feng, S.; Qin, S.; Zhang, T. Heteronanostructural Metal Oxide-Based Gas Microsensors. *Microsystems Nanoeng.* **2022**, *8*, 1–22. [CrossRef] [PubMed]
21. Song, E.; Choi, J.W. Conducting Polyaniline Nanowire and Its Applications in Chemiresistive Sensing. *Nanomaterials* **2013**, *3*, 498–523. [CrossRef] [PubMed]
22. Schwartz, I.T.; Jonke, A.P.; Josowicz, M.; Janata, J. Effect of Structured Atomic Gold on Electrooxidation of Alcohols in Alkaline Medium. *Catal. Letters* **2013**, *143*, 777–782. [CrossRef]
23. Chakraborty, P.; Chien, Y.A.; Chiu, W.T.; Chang, T.F.M.; Sone, M.; Nakamoto, T.; Josowicz, M.; Janata, J. Design and Development of Amperometric Gas Sensor with Atomic Au-Polyaniline/Pt Composite. *IEEE Sens. J.* **2020**, *20*, 12479–12487. [CrossRef]
24. Chakraborty, P. Amperometric Gas Sensor with Atomic Gold Decorated Polyaniline-Platinum Composite. Ph.D Thesis, Department of Information and Communications Engineering, Tokyo Institute of Technology, Tokyo, Japan, 2020.
25. Chakraborty, P.; Faricha, A.; Okamoto, K.; Kawakami, H.; Chang, T.-F.M.; Sone, M.; Nakamoto, T. Towards Planar Atomic-Gold Decorated Polyaniline Gas Sensors for Enhanced Electrochemical Sensing. *IEEE Sens. J.* **2023**, *23*, 6481–6488. [CrossRef]
26. Chakraborty, P.; Chien, Y.A.; Chang, T.F.M.; Sone, M.; Nakamoto, T. Indirect Sensing of Lower Aliphatic Ester Using Atomic Gold Decorated Polyaniline Electrode. *Sensors* **2020**, *20*, 3640. [CrossRef]
27. Faricha, A.; Yoshida, S.; Chakraborty, P.; Okamoto, K.; Chang, T.F.M.; Sone, M.; Nakamoto, T. Array of Miniaturized Amperometric Gas Sensors Using Atomic Gold Decorated Pt/PANI Electrodes in Room Temperature Ionic Liquid Films. *Sensors* **2023**, *23*, 4132. [CrossRef]
28. Paul, A.; Muthukumar, S.; Prasad, S. Review—Room-Temperature Ionic Liquids for Electrochemical Application with Special Focus on Gas Sensors. *J. Electrochem. Soc.* **2020**, *167*, 037511. [CrossRef]
29. Gunawan, C.A.; Ge, M.; Zhao, C. Robust and Versatile Ionic Liquid Microarrays Achieved by Microcontact Printing. *Nat. Commun.* **2014**, *5*, 3744. [CrossRef] [PubMed]
30. Gondosiswanto, R.; Hibbert, D.B.; Fang, Y.; Zhao, C. Redox Recycling Amplification Using an Interdigitated Microelectrode Array for Ionic Liquid-Based Oxygen Sensors. *Anal. Chem.* **2018**, *90*, 3950–3957. [CrossRef] [PubMed]
31. Plechkova, N.V.; Seddon, K.R. Applications of Ionic Liquids in the Chemical Industry. *Chem. Soc. Rev.* **2008**, *37*, 123–150. [CrossRef] [PubMed]
32. Amiri, V.; Roshan, H.; Mirzaei, A.; Neri, G.; Ayesh, A.I. Nanostructured Metal Oxide-Based Acetone Gas Sensors: A Review. *Sensors* **2020**, *20*, 3096. [CrossRef] [PubMed]
33. Jia, Y.; He, L.; Guo, Z.; Chen, X.; Meng, F.; Luo, T.; Li, M.; Liu, J. Preparation of Porous Tin Oxide Nanotubes Using Carbon Nanotubes as Templates and Their Gas-Sensing Properties. *J. Phys. Chem. C* **2009**, *113*, 9581–9587. [CrossRef]
34. Imae, T.; Rahmawati, A.; Berhe, A.M.; Kebede, M.A. Au Quantum Clusters and Plasmonic Quantum Nanoparticles Synthesized under Femtosecond-Pulse Laser Irradiation in Aqueous Solution and in ZIF-8 for Catalytic Reduction of 4-Nitrophenol. *ACS Appl. Nano Mater.* **2022**, *5*, 16842–16852. [CrossRef]
35. Liu, L.; Corma, A. Metal Catalysts for Heterogeneous Catalysis: From Single Atoms to Nanoclusters and Nanoparticles. *Chem. Rev.* **2018**, *118*, 4981–5079. [CrossRef]
36. Zare, E.N.; Makvandi, P.; Ashtari, B.; Rossi, F.; Motahari, A.; Perale, G. Progress in Conductive Polyaniline-Based Nanocomposites for Biomedical Applications: A Review. *J. Med. Chem.* **2020**, *63*, 1–22. [CrossRef]
37. Chani, M.T.S.; Karimov, K.S.; Khalid, F.A.; Moiz, S.A. Polyaniline Based Impedance Humidity Sensors. *Solid State Sci.* **2013**, *18*, 78–82. [CrossRef]
38. Janata, J.; Nakamoto, T. Vision of New Olfactory Sensing Array. *IEEJ Trans. Electr. Electron. Eng.* **2016**, *11*, 261–267. [CrossRef]
39. Chakraborty, P.; Kawakami, H.; Faricha, A.; Chang, T.-F.M.; Sone, M.; Nakamoto, T. Polyaniline-Atomic Au Modified Platinum Electrode with Ionic Liquid as Configuration for Enhanced Electrochemical Sensing. In Proceedings of the 2021 IEEE Sensors, Sydney, Australia, 31 October–3 November 2021; pp. 1–4.
40. Faricha, A.; Chakraborty, P.; Okamoto, K.; Chang, T.F.M.; Sone, M.; Nakamoto, T. Microgravimetric and Amperometric Sensor Coated with Room Temperature Ionic Liquid to Enhance Butanol Isomers Gas Separation. *IEEE Sens. J.* **2022**, *22*, 24471–24478. [CrossRef]
41. Figaro 5042. Available online: https://www.figarosensor.com/product/docs/tgs5042_productinfomation(fusa)_rev07.pdf (accessed on 20 June 2023).
42. Alphasense. Available online: https://cdn.shopify.com/s/files/1/0406/7681/files/DataSheet-AlphaSense-O2-A3-Oxygen-Sensor.pdf?v=1621008788 (accessed on 20 June 2023).

43. Alphasense O_2. Available online: https://www.alphasense.com/leak-free-o2/ (accessed on 20 June 2023).
44. Hayes, R.; Warr, G.G.; Atkin, R. Structure and Nanostructure in Ionic Liquids. *Chem. Rev.* **2015**, *115*, 6357–6426. [CrossRef]
45. McFarlane, D.R.; Sun, J.; Golding, J.; Meakin, P.; Forsyth, M. High Conductivity Molten Salts Based on the Imide Ion. *Electrochim. Acta* **2000**, *45*, 1271–1278. [CrossRef]
46. Manna, S.S.; Bhauriyal, P.; Pathak, B. Identifying Suitable Ionic Liquid Electrolytes for Al Dual-Ion Batteries: Role of Electrochemical Window, Conductivity and Voltage. *Mater. Adv.* **2020**, *1*, 1354–1363. [CrossRef]
47. Zhang, Y.; Shi, C.; Brennecke, J.F.; Maginn, E.J. Refined Method for Predicting Electrochemical Windows of Ionic Liquids and Experimental Validation Studies. *J. Phys. Chem. B* **2014**, *118*, 6250–6255. [CrossRef] [PubMed]
48. O'Mahony, A.M.; Silvester, D.S.; Aldous, L.; Hardacre, C.; Compton, R.G. Effect of Water on the Electrochemical Window and Potential Limits of Room-Temperature Ionic Liquids. *J. Chem. Eng. Data* **2008**, *53*, 2884–2891. [CrossRef]
49. Melián-Cabrera, I. Catalytic Materials: Concepts To Understand the Pathway to Implementation. *Ind. Eng. Chem. Res.* **2021**, *60*, 18545–18559. [CrossRef]
50. Saheb, A.; Smith, J.A.; Josowicz, M.; Janata, J.; Baer, D.R.; Engelhard, M.H. Controlling Size of Gold Clusters in Polyaniline from Top-down and from Bottom-Up. *J. Electroanal. Chem.* **2008**, *621*, 238–244. [CrossRef]
51. Fernández, E.M.; Soler, J.M.; Garzón, I.L.; Balbás, L.C. Trends in the Structure and Bonding of Noble Metal Clusters. *Phys. Rev. B-Condens. Matter Mater. Phys.* **2004**, *70*, 165403. [CrossRef]
52. Häkkinen, H.; Landman, U. Gold Clusters and Their Anions. *Phys. Rev. B-Condens. Matter Mater. Phys.* **2000**, *62*, R2287–R2290. [CrossRef]
53. Schwartz, I.; Jonke, A.P.; Josowicz, M.; Janata, J. Polyaniline-Supported Atomic Gold Electrodes: Comparison with Macro Electrodes. *Catal. Lett.* **2012**, *142*, 1344–1351. [CrossRef]
54. Songkhla, S.N.; Nakamoto, T. Overview of Quartz Crystal Microbalance Behavior Analysis and Measurement. *Chemosensors* **2021**, *9*, 350. [CrossRef]
55. Aleixandre, M.; Nakamoto, T. Study of Room Temperature Ionic Liquids as Gas Sensing Materials in Quartz Crystal Microbalances. *Sensors* **2020**, *20*, 4026. [CrossRef] [PubMed]
56. He, L.; Jia, Y.; Meng, F.; Li, M.; Liu, J. Development of Sensors Based on CuO-Doped SnO_2 Hollow Spheres for Ppb Level H_2S Gas Sensing. *J. Mater. Sci.* **2009**, *44*, 4326–4333. [CrossRef]
57. Oh, J.; Kim, Y.K.; Lee, J.S.; Jang, J. Highly Porous Structured Polyaniline Nanocomposites for Scalable and Flexible High-Performance Supercapacitors. *Nanoscale* **2019**, *11*, 6462–6470. [CrossRef] [PubMed]
58. Nozaki, Y.; Nakamoto, T. An Olfactory Sensor Array for Predicting Chemical Odor Characteristics from Mass Spectra with Deep Learning. In *Methods Molecular Biology*; Humana: New York, NY, USA, 2019; Volume 2027, pp. 29–47. [CrossRef]
59. Tan, J.; Xu, J. Applications of Electronic Nose (e-Nose) and Electronic Tongue (e-Tongue) in Food Quality-Related Properties Determination: A Review. *Artif. Intell. Agric.* **2020**, *4*, 104–115. [CrossRef]
60. Nakamoto, T. *Human Olfactory Displays and Interfaces: Odor Sensing and Presentation*; IGI Global: Hershey, PA, USA, 2012.